Pharmaceutical Research, Vol. 6, No. 7, 1989

Review

Current Aspects of Practical Two-Dimensional (2D) Nuclear Magnetic Resonance (NMR) Spectroscopy: Applications to Structure Elucidation

Richard W. Kriwacki[1] and T. Phil Pitner[1,2]

Received; accepted

The intense effort in developing new 2D NMR methodology over the past decade has been driven by the desire to study molecules of progressively greater complexity. The need for refined structural detail has produced new types of experiments that require more involvement on the part of the practicing spectroscopist in understanding the theoretical bases leading to their experimental realization. In this Review we discuss several concepts that are important in the successful application of current versions of the most useful 2D NMR experiments, such as coherence transfer, phase cycling, apodization functions, and obtaining pure-phase 2D NMR spectra. The intimate interconnections among these concepts are emphasized. The principles underlying the 2D NMR experiments are described and then the experiments are illustrated in assigning the ^{1}H and ^{13}C NMR spectra of the triterpene, ursolic acid.

KEY WORDS: Nuclear magnetic resonance (NMR); two-dimensional (2D) NMR; pulse sequence; phase cycle; COSY; double-quantum filtered COSY; CH COSY; indirect detection; NOESY; relayed COSY; TOCSY; HOHAHA; ROESY.

INTRODUCTION

In the time period since the first two-dimensional nuclear magnetic resonance (2D NMR) experiment was suggested by Jeener (1) and then demonstrated (2,3), the field has developed from an area perceived initially as esoteric, to one in which daily routine application of the methodology is made by an increasing number of NMR laboratories. Since excellent, complete, current reviews and texts exist covering this topic (4–12), it is not the goal of this Review to provide a comprehensive overview of all the past literature. It is our intent to present the subject from the point of view of practicing NMR spectroscopists, covering those topics with which the spectroscopist involved in mainly 1D NMR may not be familiar and omitting those aspects covered fully in basic texts on pulse FTNMR such as that by Farrar and Becker (13). In the first part of this Review, we concentrate on several concepts that are pertinent to acquiring and processing 2D NMR data, presented in the context of the most commonly used experiments in the most recent versions.

In the second part of this Review, each technique is demonstrated in assigning the ^{1}H and ^{13}C NMR spectra of the triterpene, ursolic acid (1). Although the structure of this compound is well-known and it and related compounds have been analyzed to some extent by NMR (14–16), it provides an excellent example of the sequence in which 2D NMR experiments are applied.

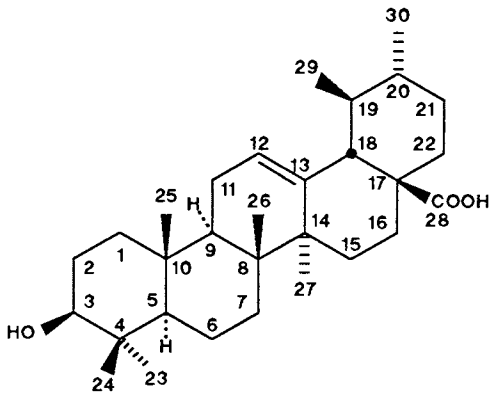

1

Scheme 1

WHY 2D NMR?

The power of NMR in structure elucidation derives in large part from its ability to establish bonding connectivity (via J-coupling interactions) or through-space proximity (via dipolar coupling interactions) of nuclei. The amount of time consumed in elucidating a structure depends on the rate at which these interactions can be detected by NMR and analyzed. 1D NMR methods most often explore interactions between only a few nuclei at a time: spin–spin decoupling

[1] Boehringer Ingelheim Pharmaceuticals, Inc., 90 East Ridge, Ridgefield, Connecticut 06877.

[2] To whom correspondence should be addressed.

0724-8741/89/0700-0531$06.00/0

measurements are used to demonstrate through-bond connectivity; and NOE measurements are used to probe internuclear distances. In the corresponding 2D NMR experiments, many J-coupling interactions (COSY) (COrrelation SpectroscopY) (1) or dipolar interactions (NOESY) (Nuclear Overhauser Effect SpectroscopY) (17) are demonstrated simultaneously; therefore, for complex molecules, 2D NMR experiments provide much more structural information in a given time period. In order to select the type of interaction that will be detected, a specific sequence of rf pulses separated by delays (pulse sequence) is applied to the nuclei.

EXPERIMENTAL

Ursolic acid was purchased from Sigma Chemical Company, and 5-bromoindole from Aldrich Chemical Company. For NMR analysis, the compounds were dissolved in DMSO-d_6 (5-bromoindole 0.2*M*) or pyridine-d_5 (ursolic acid, 80 m*M*) obtained from Aldrich Chemical Company. ^{1}H (270.13 MHz) and ^{13}C (67.92 MHz) spectra were obtained with a Bruker AC-270 NMR spectrometer. Experimental details are presented in the figure legends. All spectra except the ^{1}H-detected CH COSY and the HOHAHA spectra were obtained with an ASPECT 3000 computer equipped with a Bruker Pulse Programmer; because of the complicated pulse sequences required for decoupling ^{13}C and for spin-locking, these two experiments were executed with an ASPECT 3000 equipped with the Bruker Process Controller.

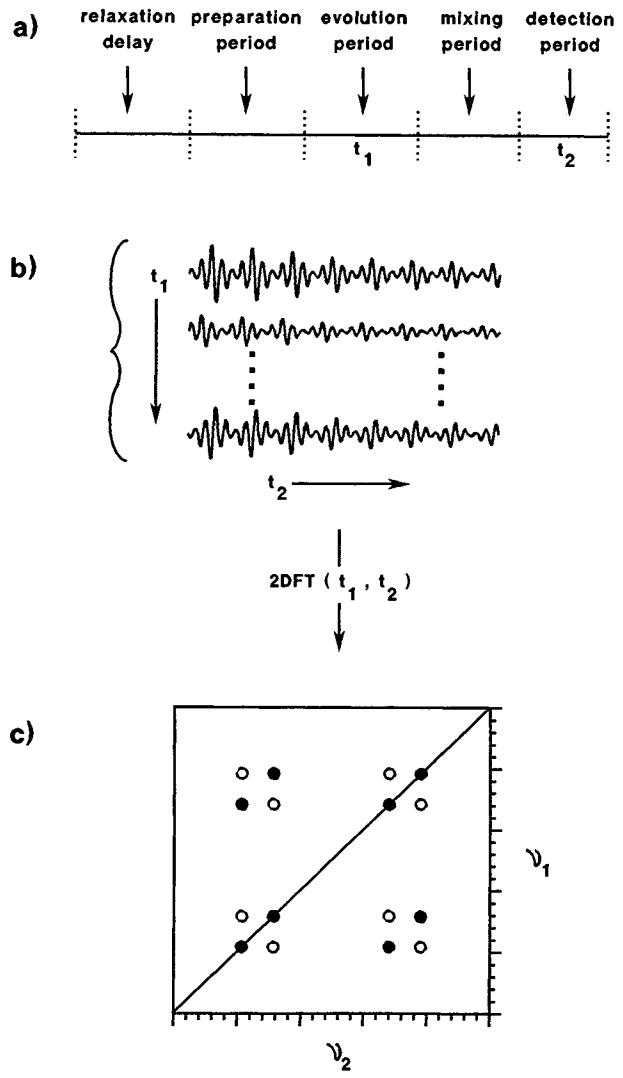

Fig. 1. Schematic representation of the typical 2D NMR experiment showing (a) standard nomenclature, (b) time domain data, and (c) a contour plot of frequency domain data.

THE 2D NMR EXPERIMENT

The 2D NMR experiment is divided into several parts (Fig. 1) as first described by Aue *et al.* (3). During the *relaxation delay,* the nuclear spins return to thermal equilibrium. The *preparation period* serves to "prepare" the spins in a desired nonequilibrium state and usually consists of some combination of pulses and/or delays. This is done so that during the *evolution period* (t_1) an NMR property(ies) of the nuclei (e.g., chemical shift, J-coupling) can evolve with time. The *mixing period,* consisting of pulses and/or delays, serves to transfer information about the properties of one nucleus (properties that were causing evolution of the spin system during the evolution period) to the intensity and/or phase of signals of another nucleus observed during the *detection period* (t_2).

For example, in COSY (1) chemical shift information of one nucleus, that was evolving during t_1, is transferred by a $\pi/2$ mixing pulse into phase and intensity information of the peaks of a J-coupled nucleus. To obtain a 2D spectrum, a series of spectra is acquired with all experimental parameters the same, except the t_1 delay, which is varied incrementally as the series progresses (Fig. 1b). Fourier transformation with respect to t_2 produces a series of spectra that appear normal except that the phases and intensities of the peaks have been modulated by the chemical shifts and J-coupling constants of other nuclei belonging to the same J-coupled spin system. A second Fourier transformation (with respect to t_1) produces a 2D spectrum with two frequency axes (Fig. 1c).

In the most common presentation of 2D NMR data, the contour plot (Fig. 1c), the interactions between nuclei result in cross-peak contours at frequency coordinates (ν_1,ν_2) corresponding to the chemical shifts of the two interacting nuclei.

COHERENCE TRANSFER

A key concept in many 2D NMR experiments is coherence transfer, by which spin-coupled nuclei, under the influence of an rf pulse(s), interchange information. Coherence transfer can be explained elegantly using either the density matrix (18), or the product operator (19) formalism, both of which are outside the scope of this review. However, since coherence transfer is essential to later discussion, we provide here a short conceptual description. These ideas are discussed in the context of COSY (Fig. 2). We use the common graphic representation of pulse sequences depicted in Fig. 2.

Consider two nuclei A and B that are J-coupled with a coupling constant J_{AB}. Before the first $\pi/2$ pulse, the A magnetization is aligned along the z axis (longitudinal magnetization). The first $\pi/2$ pulse (preparation period) converts the

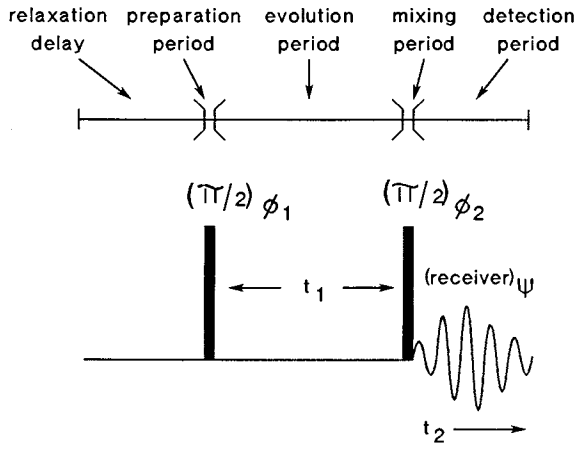

Fig. 2. Pulse sequence for 2D homonuclear correlation spectroscopy (COSY).

longitudinal A magnetization into in-phase A magnetization (refer to Fig. 3 during the discussion of coherence transfer).

$$\text{Longitudinal}_A \xrightarrow{\pi/2} \text{In-phase}_A \qquad \textit{Preparation}$$

In the vector diagram formalism, in-phase A magnetization corresponds to the situation in which the two magnetization vectors of A (due to J-coupling with B) are aligned pointing in the same direction in the xy plane. During the evolution period t_1, the in-phase A magnetization is converted into antiphase A magnetization under the influence of the coupling J_{AB} and at a rate dependent on $1/J_{AB}$.

$$\text{In-phase}_A \xrightarrow{J_{AB}} \text{Antiphase}_A \qquad \textit{Evolution}$$

In the vector diagram picture, this evolution corresponds to the "fanning-out" of the two magnetization vectors of the A nucleus. Antiphase A magnetization corresponds to the situation in which the two magnetization vectors of A are aligned in an antiparallel manner, pointing in opposite directions in the xy plane. Although the effect of the next step can be shown using vecor diagrams, the vector diagram formalism cannot actually predict the result. This step is the important coherence transfer process, in which antiphase A magnetization is converted into antiphase B magnetization under the influence of the second $\pi/2$ pulse.

$$\text{Antiphase}_A \xrightarrow{\pi/2} \text{Antiphase}_B \qquad \textit{Mixing}$$

Except in very special circumstances, antiphase magnetization (antiphase coherence) must exist for coherence transfer to occur; in-phase A magnetization (in-phase coherence) is nutated in the same manner as classical magnetization vectors by a pulse, with no coherence transfer occurring. Although not explicitly shown in the expression describing evolution, the chemical shift of nucleus A is also evolving during t_1, causing a periodic oscillation in the magnitude of antiphase transfer from A to B. This can be seen more clearly in Fig. 3. If the second $\pi/2$ pulse is applied along x, it is only the y component of the antiphase A magnetization that is transferred to antiphase B magnetization. Since the magnitude of this y component is dependent on the chemical shift of A, the magnitude of the resultant antiphase B magnetization will also be dependent on the chemical shift of A.

After the mixing pulse, the antiphase B magnetization evolves into observable in-phase B magnetization due to J_{AB} and is detected during t_2.

$$\text{Antiphase}_B \xrightarrow{1/J_{AB}} \text{In-phase}_B \qquad \textit{Detection}$$

The oscillation in the intensity of the y-antiphase B magnetization due to the chemical shift of A produces peaks in the ν_1 dimension of the 2D plot. Of course, a simultaneous process occurs involving transfer from B to A. These coherence transfers produce the off-diagonal peaks (cross-peaks) in the COSY spectrum and are diagnostic of J-coupling between nuclei at the corresponding chemical shifts along each axis

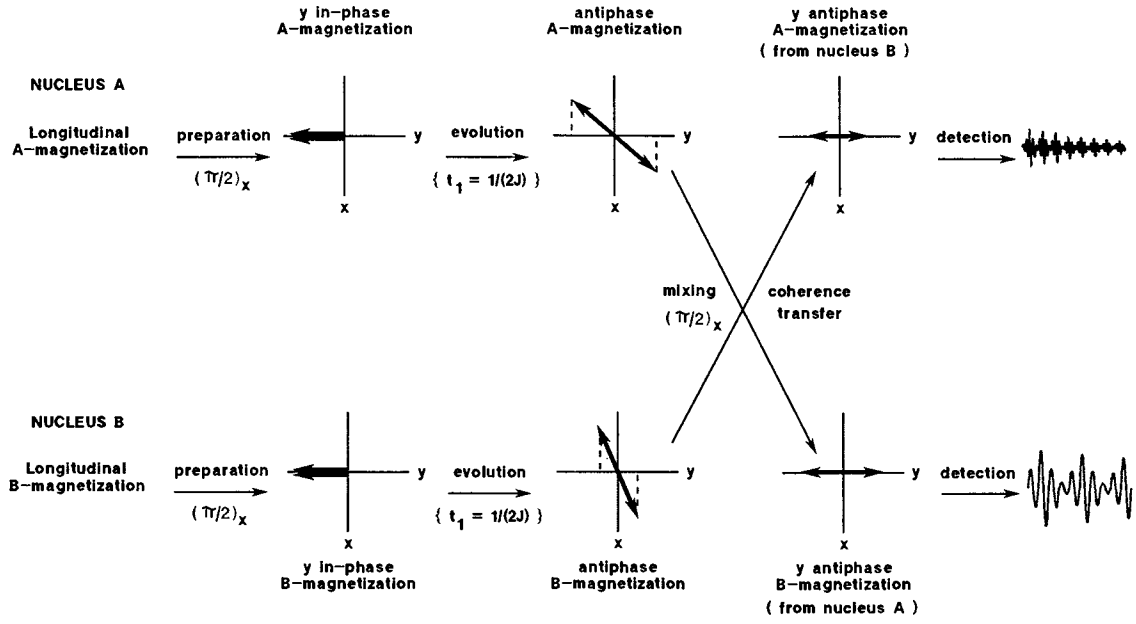

Fig. 3. Schematic representation of the coherence transfer process involved in COSY.

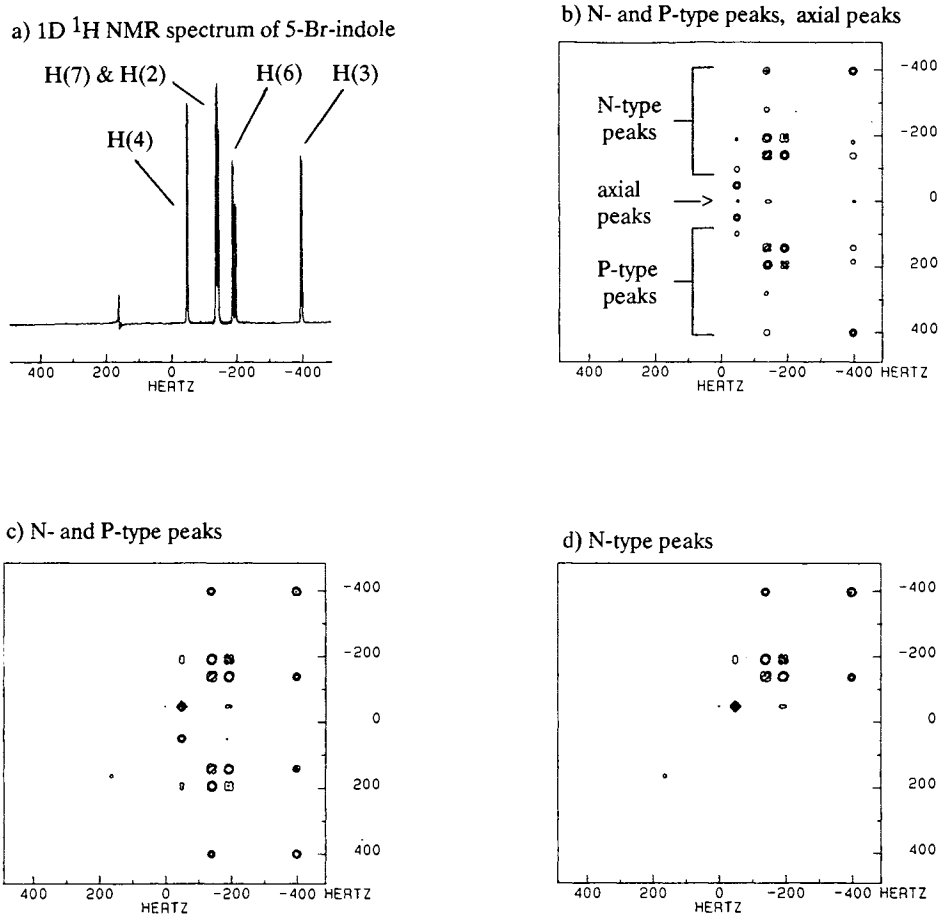

Fig. 4. COSY spectra of 5-bromoindole in DMSO-d_6, illustrating artifacts which result from inadequate phase cycling. rf carrier at low-field end of spectrum; quadrature detection (ν_2); sine-bell apodization in both dimensions; absolute-value mode; 256 points × 256 points data, zero filled to 512 × 512. (a) 1D NMR spectrum of 5-bromoindole for reference; (b) no phase cycling; (c) phase cycling as described in the text to remove axial peaks; (d) phase cycling to remove axial peaks and select N-type peaks.

(Fig. 4). For a very complete and lucid treatment of coherence transfer (as well as other phenomena important in 2D NMR), the reader is referred to the article that describes the product operator formalism by Sørensen *et al.* (19).

The relationships among the various types of doublet-magnetization, their FIDs (Free Induction Decay), and the resulting 1D spectra are shown in Fig. 5. In the FIDs, the interchange between in-phase (vectors parallel) and antiphase (vectors antiparallel) magnetization can be seen as the signals pass through maxima and minima about four times due to J-coupling. The more rapid oscillation is due to chemical shift. The y magnetization that is in-phase at the beginning of the FID produces an absorptive in-phase doublet; whereas the y magnetization that is antiphase at the beginning of the FID produces an absorptive antiphase doublet. The x magnetization produces dispersive doublets. Of course, it is an arbitrary convention to represent y (rather than x) as the axis along which magnetization produces absorptive peaks, since in conventional 1D NMR, the final spectrum can be adjusted to absorption in either case.

ACQUIRING AND PROCESSING A 2D SPECTRUM

Here we present concepts common to acquiring and processing all types of 2D NMR spectra. We describe such ideas as phase cycling, quadrature detection in t_1, the effects of apodization functions, and pure-phase detection. There are aspects of each of these topics that are interdependent, making it impossible to discuss a single topic without some consideration of at least one of the others.

Phase Cycling

Almost always, the final FID for each value of t_1 represents the sum of several scans, each acquired with different relative phases of the rf pulses; the relative phase of the receiver (ψ) is varied as well. This "phase cycling" gives the specroscopist greater control over the 2D NMR experiment: the nuclear spins can be manipulated in order to observe only peaks that reflect the desired internuclear interaction and to suppress undesired peaks, instrumental artifacts can also be suppressed, and the final data presentation can be

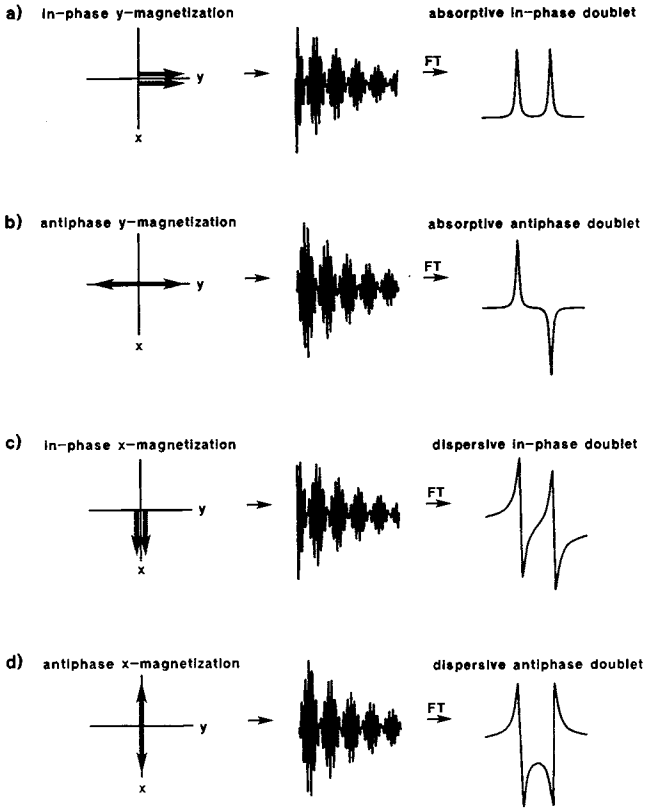

Fig. 5. Schematic representations of "in-phase" and "antiphase" transverse magnetization showing the vector representation, the corresponding FIDs, and Fourier-transformed spectra.

controlled. We use the common notation for the pulse phases, which denotes them by reference to the axis of the rotating frame along which the B_1 field (rf pulse) is applied. This, of course, will not suffice for pulses shifted in non-90° increments as used in some newer experiments but not available on most existing spectrometers. In most spectrometers the receiver is technically not phase cycled, but the effect of a 90° phase shift is achieved by interchanging the two quadrature channels (that are 90° out of phase) and adding to or subtracting from computer memory.

To underscore the essential roles of phase cycling, 2D COSY spectra of 5-bromoindole were obtained with selected

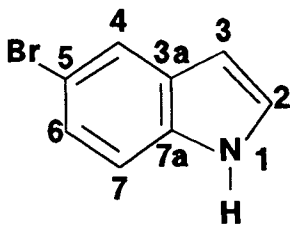

2

Scheme II

phase cycles (Fig. 4). For purposes of illustration, the carrier frequency was set to the low-field side of the ^1H peaks and quadrature detection was used in acquiring the FIDs.

The series of FIDs used to produce the spectrum in Fig. 4b were all obtained without phase cycling to illustrate the artifacts that arise in cases of nonoptimal phase cycles. Note that along a horizontal line at 0 Hz in the ν_1 dimension, peaks appear in the COSY spectrum at positions corresponding to ^1H NMR chemical shifts in the ν_2 dimension. These so-called "axial peaks" (20,21) are a nuisance and can complicate interpretation of crowded spectra by obscuring cross-peaks. They correspond to magnetization that did not evolve during t_1, such as M_z that develops during t_1 due to spin-lattice relaxation. These axial peaks may be effectively eliminated by phase cycling the second pulse in the COSY sequence (Fig. 2b) between x and $-x$.

ϕ_1	ϕ_2	ψ
x	x	x
x	$-x$	x

Scheme III

Coaddition of the two scans obtained in this manner cancels the signals resulting from the M_z component, since these signals would be of opposite sign for these two scans; however, the signals that result from coherence transfer between nuclei are not affected by the phase reversal and, hence, contribute to cross-peaks in the final spectrum (Fig. 4c). Peaks that have the same ν_1 and ν_2 coordinates (diagonal peaks) are also not affected by this phase cycle.

In Figs. 4b and c, the 2D NMR spectrum appears in both the upper and the lower right quadrants, in mirror image about the $\nu_1 = 0$ line. This is similiar to the folding that occurs in 1D NMR if the rf carrier is improperly placed within the spectrum. The sets of peaks in the lower quadrant are known as "P"-type peaks and those in the upper are known as "N"-type peaks (21) and result from the inability of the two-step phase cycle to distinguish the sense of precession (positive or negative) of specific magnetizations during t_1. This makes intuitive sense from one's experience with 1D NMR: quadrature detection requires that magnetization be sampled along both the x and the y axes to determine the sense of precession of magnetization. The second pulse (phase $x, -x$) samples along only one of these orthogonal axes at the end of t_1; therefore, the sense of precession during t_1 cannot be determined with this phase cycle. The presence of both sets of peaks would preclude placing the rf carrier in the center of the spectrum, since peaks on both sides of the carrier would fold about the center, producing overlap.

To determine the sense of precession during t_1, the phase of the second $\pi/2$ pulse is cycled between x and y in order to sample magnetization along both orthogonal axes at the end of t_1. Coaddition or subtraction of these two scans and subsequent Fourier transformation (with respect to t_2) produces a series of spectra, in which the phase of the individual resonances oscillate in t_1 with frequencies equal to the chemical shifts of all nuclei in the J-coupled spin system. These "phase-modulated" signals can then be subjected to complex Fourier transformation (with respect to t_1) to determine the sense of rotation in the rotating frame. Subtraction of these two scans (phase cycling the receiver between $+x$ and $-x$) selects the N-type signals (Fig. 4d). In effect, N-

type signals precess in opposite senses during t_1 and t_2 due to this cycling of the receiver phase; P-type peaks, on the other hand, in effect, precess in the same sense in t_1 and t_2, since to select these peaks, the receiver phase is constant. (Of course, the actual sense of precession of the magnetization vectors cannot be altered by phase cycling, but cycling the receiver between x and $-x$ produces this illusion in the detected signal.) The lineshapes arising from N- and P-type peaks have been shown theoretically (7) to be different for small molecules, the resolution being better for the N-type. For this reason N-type peaks are normally selected. The two types of phase cycling just mentioned (for the elimination of axial peaks and N-type peak selection) can be nested into a four-element cycle.

ϕ_1	ϕ_2	ψ		
x	x	x	N-type peak selection	Axial peak elimination
x	y	$-x$		
x	$-x$	x		
x	$-y$	$-x$		

Scheme IV

These types of phase cycling involve manipulation of the nuclear spins to remove axial peaks and produce "quadrature detection" in ν_1. Additional artifacts, however, result from instrumental imperfections and may obscure real information in the 2D NMR spectra. It is a familiar notion to the NMR spectroscopist that an amplitude imbalance between the two quadrature channels will produce "images" in the spectrum, consisting of a smaller set of peaks located at mirror-image positions about the rf carrier. In addition, a DC offset in either or both of these channels will result in a spike located at the carrier position. Analogous artifacts may be produced in the ν_2 dimension of the 2D NMR spectrum. They are not visible in Fig. 4 because the balance between the two quadrature channels has been carefully adjusted; however, they might become a problem if large peaks (e.g., methyl singlets) were present in the spectrum. The artifacts

ϕ_1	ϕ_2	Ψ			
x	x	x	N-type peaks	Axial peak elimination	CYCLOPS
x	y	$-x$			
x	$-x$	x			
x	$-y$	$-x$			
y	y	y			
y	$-x$	$-y$			
y	$-y$	y			
y	x	$-y$			
$-x$	$-x$	$-x$			
$-x$	$-y$	x			
$-x$	x	$-x$			
$-x$	y	x			
$-y$	$-y$	$-y$			
$-y$	x	y			
$-y$	y	$-y$			
$-y$	$-x$	y			

Scheme V

are removed by incrementing the pulse and receiver phases by 90° in concert, a technique known as CYCLOPS (CYCLically Ordered Phase Sequence) (22). Since, as mentioned above, the 90° receiver phase shift is accomplished by interchanging the two quadrature channels and appropriately adding to or subtracting from memory, this phase cycling technique averages any imbalance between the two channels and removes DC offset during the steps requiring subtraction. The final phase cycle for COSY in which all of the cycles discussed so far are incorporated is shown in Scheme V. Indicated to the right of the cycle are the critical steps responsible for each subfunction performed by the cycle. This nesting of phase cycles produces a 16-step cycle ($2 \times 2 \times 4 = 16$).

With this phase cycle the rf carrier may be set in the middle of the spectrum, allowing quadrature detection in both the ν_1 and the ν_2 dimensions, taking advantage of more efficient use of pulse power and smaller data sets. Shown in Fig. 6a is the 2D NMR COSY spectrum of 2 obtained with no phase cycling and the rf carrier placed in the middle of the spectrum. Folding of the spectrum about ν_1 = carrier frequency (ca. −250 Hz) occurs, and axial peaks are clearly visible along this line. (For clarity, the chemical shift scale in Fig. 6 is kept the same as in Fig. 4.) With the 16-step cycle, these artifacts are removed (Fig. 6b). In this Review, we use the convention shown for plotting the spectra acquired with N-type selection, with the diagonal running from lower left to upper right.

The systematic design of phase cycles using a concept known as "coherence levels" has been described in the literature (23,24), and these references are recommended to the reader who is interested in pursuing this topic in greater detail.

Apodization Functions

Apodization functions are commonly used in 1D NMR (25). Multiplying an FID by a function that decreases with time, such as a decaying exponential, may be used to increase the spectral signal-to-noise ratio (S/N), whereas multiplication by a function that increases with time, such as a rising exponential, can be used to enhance the resolution of closely spaced peaks at the expense of degraded S/N. Optimized functions that have the properties of initially increasing with time and then decreasing can be used to enhance resolution, while simultaneously maintaining some control over S/N; the sine-bell function and Lorentz/Gauss function are of this type.

The same considerations apply to 2D NMR, except that apodization functions assume additional important roles. The spectra shown so far are acquired in what is called the "non-pure-phase" mode (this is clarified below under Quadrature Detection in t_1 with Pure-Phase Lineshapes) and are plotted in the absolute value presentation. To calculate an absolute-value spectrum in 1D NMR, one would use the following function.

$$S(\nu) = \sqrt{\mathrm{Re}^2(\nu) + \mathrm{Im}^2(\nu)}$$

In an unphased 1D spectrum, the real (Re) and imaginary

a) No phase-cycling, sine-bell apodization, absolute-value mode

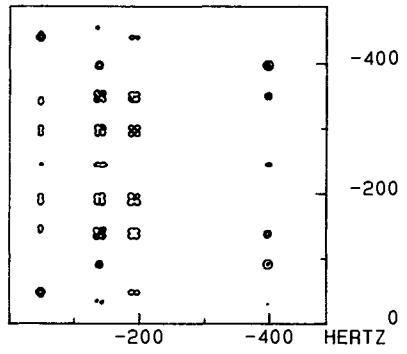

b) "Axial peak" elimination, "N"-type peak selection, sine-bell apodization

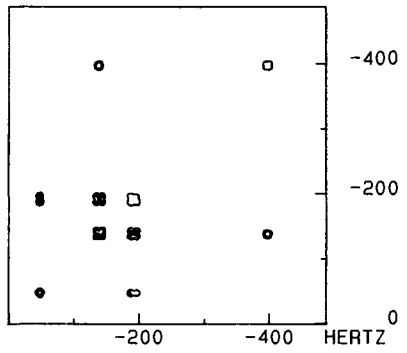

c) "Axial peak" elimination, "N"-type peak selection, no apodization

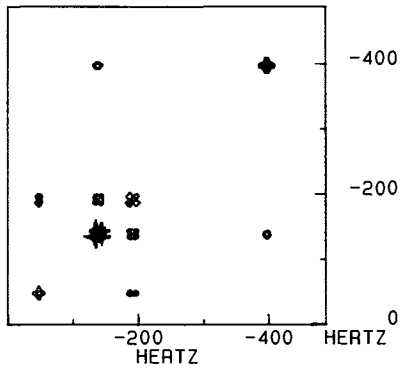

Fig. 6. COSY spectra of 5-bromoindole. rf carrier in middle of spectrum; quadrature detection (ν_2); absolute-value mode; 256 × 256 points, zero filled to 512 × 512. (a) No phase cycling, sine-bell apodization in both dimensions; (b) phase cycling to remove axial peaks and select N-type peaks, sine-bell apodization in both dimensions; (c) phase cycling to remove axial peaks and select N-type peaks, no apodization. The chemical shift scale is the same as in Fig. 4.

(Im) are composed of a mixture of absorptive and dispersive components; however, in a properly phased 1D spectrum, the real (Re) part is absorptive and the imaginary (Im) part is dispersive. Because the Im component has such wide tails, the 1D plot of $S(\nu)$ produces a spectrum in which the peaks have very wide tails (Fig. 7a). Fortunately, in 1D NMR one has the option of plotting only the Re absorptive part.

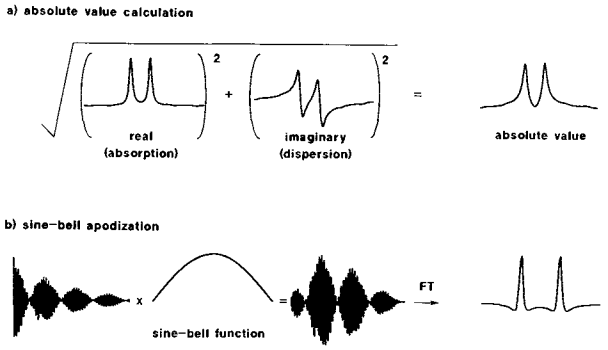

Fig. 7. Illustration of the effect of (a) absolute-value calculation and (b) sine-bell apodization on resonance lineshape.

In the method described above for obtaining quadrature detection in t_1, no such option exits. Due to the manner in which the data are acquired, the Re and Im parts are both composed of a mixture of absorptive and dispersive components that are inextricable. The resultant "phase-twist" lineshape (26,27) cannot be phase corrected to pure absorption. Therefore, spectra are plotted in the absolute value mode. With no apodization, this leads to peaks with broad bases (as above in 1D NMR) forming a star pattern (Fig. 6c). The use of certain apodization functions can ameliorate this difficulty to some degree. In particular, functions such as the pseudo-echo (28), sine-bell (29), and squared sine-bell (8) will "push down" the tails of these base-broadened spectra (Fig. 7b), since these functions are symmetric and remove contributions from the dispersive component (5,7). A similar effect is seen in 1D NMR: excessive application of such functions often produces troughs at the sides of sharp peaks (Fig. 7b). Just as in 1D NMR, the use of these functions can lower sensitivity due to the reduction of signal at the beginning of the FID. Additionally, these functions can cause intensity distortions when the spectrum contains peaks of different widths. Functions such as the shifted sine-bell and Lorentz/Gauss can be tailored to provide a compromise between resolution and sensitivity (25).

For a complete treatment of apodization functions presented in the context of 1D NMR, the reader is referred to the review article by Lindon and Ferrige (25).

t_1 Noise

A feature of 2D NMR spectra that is often observed in studies of molecules having large peaks, such as CH_3 singlets, is noise stripes extending along the ν_1 dimension, passing through these peaks. These so-called t_1 "tails" result from imperfect reproducibility of spectrometer performance and from failure to achieve a steady-state nuclear population before each acquisition (30,31). This produces a random variation of signal amplitude that Fourier transforms to bands of t_1 noise.

To minimize t_1 noise, the magnetic field must be as stable as possible throughout the acquisition of data; therefore, any perturbation of the field/frequency lock must be avoided. This includes maintaining a constant probe temperature; if the lock signal has a large chemical-shift tempera-

ture dependence (such as D_2O), then slight temperature variations can cause changes in resonance positions. Also, it has been demonstrated that sample spinning can also produce t_1 "tails"; many of the spectra in this Review were obtained nonspinning. It is additionally recommended that spectrometer-controlled automatic shimming of field homogeneity not be performed during 2D NMR data acquisition, as this can often produce field instability.

To ensure that steady-state conditions exist for the nuclear spin system, the pulse sequence is often applied to the nuclear spins several times before actual data acquisition begins; in this Review, we apply at least four "dummy scans" before data acquisition. Dummy scans can be eliminated and steady state maintained if data are acquired without interruption for data storage between successive t_1 values. Alternatively, a long relaxation delay ($\gtrsim 4T_1$) can be used, but this is often not time efficient.

In contrast to the noise stripes discussed in the previous paragraphs, which consist of points displaced randomly above and below the plane of the contour plot, an additional type of noise stripe (both ν_1 and ν_2) is observed in 2D spectra. These stripes appear at constant offset above or below the plane and are therefore referred to as t_1 or t_2 ridges. One solution for minimizing these ridges involves manipulation of the processed 2D data (32). A single row is chosen that contains no spectral peaks. This row will, however, contain displacements due to the t_1 ridges that pass through it vertically. Since these same displacements will be present in each row, point-by-point subtraction of this row from all rows will diminish the contributions due to the ridges.

An alternative approach for removing t_1 and t_2 ridges involves manipulation of the FIDs prior to Fourier transformation (33), a method that can be understood by recalling that the first point in the FID determines the magnitude of the DC offset in the final spectrum. This point is multiplied by a factor (the same for all FIDs) between 0.0 and 1.0 (often $\simeq 0.5$) determined empirically to minimize these ridges. After the first Fourier transformation (with respect to t_2), a similar scaling of the first data point in each interferogram is peformed before Fourier transformation in the t_1 dimension. We have used the latter method to minimize ridges in the NOESY spectrum of 1, since in NOESY, the cross-peaks are often very small relative to diagonal peaks, so that the ridges interfere more severly.

Symmetrization

The desire to improve the appearance of and accessibility to information in 2D NMR spectra has led to methods that involve processing of data after 2D transformation. The idea for one such method, symmetrization, comes from the fact that homonuclear correlation experiments such as COSY, NOESY, and other closely related experiments theoretically yield spectra that are symmetrical about the diagonal (7); in contrast, neither random noise nor artifacts such as t_1 noise are symmetrical about the diagonal. Symmetrization refers to techniques designed to take advantage of this distinction and is approached in several ways. One of the more common involves comparing each data point with its counterpart point symmetrically located on the other side of the diagonal and giving both points the intensity value of the smaller (34). In this manner, those points that have a large intensity on only one side of the diagonal are minimized, thereby reducing random noise and t_1 noise and, hopefully, not affecting the actual 2D data. In practice, there are experimental and practical constraints that limit the cases in which symmetrization does not produce some type of distortion to the 2D data. The data are symmetrical only if they are acquired with the same digital resolution in the t_1 and the t_2 dimensions and only if identical processing parameters are used. Otherwise, effective linewidths and peakshapes will be different in the two dimensions and the symmetrized data will be distorted. Instrumental instabilities can also result in nonsymmetrical data. In the case of NOESY, nonsymmetrical data can be produced if the spin system is not at thermal equilibrium.

There is a great temptation to use symmetrization for purely cosmetic purposes, but unfortunately it can also remove weak peaks, distort data, and affect spectrum interpretation. If symmetrization is used, it is recommended that both symmetrized and nonsymmetrized data be viewed simultaneously to eliminate the possibility of misinterpretation. Symmetrization has not been applied to any spectra presented in this Review.

Quadrature Detection in t_1 with Pure-Phase Lineshapes

Because of the peakshape distortions (phase twist) introduced by the method described above for separating N- and P-type signals (quadrature detection in t_1), other approaches were sought to achieve this separation and, in addition, maintain separation of the absorptive and dispersive peak components, thereby eliminating the phase twist and providing pure absorption-mode (pure-phase) lineshapes in 2D NMR spectra. Two data acquisition and processing procedures have been developed for this purpose, the hypercomplex transform (35,36) and TPPI (time-proportional phase incrementation) (37). Since TPPI is employed in our laboratory, we describe this method. Excellent discussions of the other approach are available (36,38).

TPPI is the 2D NMR analogue of the 1D NMR approach suggested by Redfield and Kunz (39) for obtaining quadrature detection with spectrometers that had only a real Fourier transform routine. In the 1D NMR approach, the rf carrier is set in the center of the spectrum, and as the data are acquired, the phase of the receiver is incremented by 90° for each data point. Signals that precess in the same sense as the receiver phase incrementation appear to be rotating more slowly than they would with normal detection, whereas those precessing in the opposite sense appear to be rotating faster. Therefore, a peak at the high-frequency end of the spectrum would be tracked by the phase rotation exactly and would effectively not precess in the rotating frame, and a peak at the opposite end would appear to be precessing twice as fast in the opposite direction. The overall result is to make it seem as if the detector frequency were moved from the center of the spectrum to one end of the spectrum, allowing the discrimination of positive and negative frequencies.

The 2D NMR analogue of this effect is achieved with the following phase settings.

	ϕ_1	ϕ_2	ψ
FID 1	x	x	x
FID 2	y	x	x
FID 3	$-x$	x	x
FID 4	$-y$	x	x
FID 5	x	x	x
FID 6	y	x	x
.			
.			
.			
etc.			

Scheme VI

In the 1D NMR experiment described above, the phase shift of the receiver allowed tracking of events that were occurring during t_2. In the 2D NMR experiment, we wish to track events that occur during t_1, and it is necessary to produce the illusion that during t_1, the chemical shifts of nuclei at one end of the spectrum are approximately 0 Hz, while those at the other end are doubled in value. To accomplish this, each successive set of scans corresponding to a single t_1 FID is acquired with a 90° increment in the phase of the first pulse, producing a repeat of phase settings every fourth t_1 value. Since for each incremental t_1 value, the magnetization is brought into the plane 90° further in a counterclockwise direction, an additional one-fourth revolution is added to the precession of the nuclei before the t_1 evolution occurs, so that the nuclei that precess in a counterclockwise sense appear to be precessing faster, while those that precess in a clockwise sense appear to be precessing slower. This effective change in precession frequencies is transferred by the mixing pulse into the information acquired during t_2, allowing a real Fourier transform in t_1 to provide quadrature detection and simultaneously keep absorptive and dispersive

	ϕ_1	ϕ_2	ψ			
FID 1	x	x	x	Axial peak elimination	CYCLOPS	TPPI
	x	$-x$	x			
	y	y	y			
	y	$-y$	y			
	$-x$	$-x$	$-x$			
	$-x$	x	$-x$			
	$-y$	$-y$	$-y$			
	$-y$	y	$-y$			
FID 2	y	x	x			
	y	$-x$	x			
	$-x$	y	y			
	$-x$	$-y$	y			
	$-y$	$-x$	$-x$			
	$-y$	x	$-x$			
	x	$-y$	$-y$			
	x	y	$-y$			
FID 3	$-x$	x	x			
.						
.						
etc.						

Scheme VII

Table I. Peakshapes in Pure-Phase 2D NMR Experiments

Experiment	Cross-peaks	Diagonal
COSY	Absorption Antiphase	Dispersion In-phase
DQ filtered COSY	Absorption Antiphase	Absorption Antiphase
NOESY	Absorption In-phase Negative (small molecules) Positive (large molecules)	Absorption In-phase Positive
ROESY	Absorption In-phase Negative	Absorption In-phase Positive
Relayed COSY	Relay—Absorption Antiphase COSY—Mixture	Mixture
TOCSY/HOHAHA	Absorption In-phase Positive	Absorption In-phase Positive

components separate for pure-phase presentation of spectra. To aid in the phasing process, the expected types of diagonal and cross-peaks for COSY (as well as other homonuclear experiments) are shown in Table I.

To eliminate axial peaks, DC offset, and quadrature channel imbalance, the TPPI sequence is augmented by nesting additional phase cycling. 2D NMR spectra acquired using TPPI can obviously be presented in either the absolute-value or the pure-phase mode. However, they can be more sensitive to the accuracy and reproducibility of the phase and amplitudes of the rf pulses than in the original phase-modulation method. In TPPI, it is important to calibrate pulse amplitudes and phase shifts accurately, since misadjustment of these experimental parameters can produce an annoying artifact, the "antidiagonal," that runs between the upper left and the lower right corners of the 2D NMR contour plot, causing spectral clutter that is analogous to folding in 1D NMR. In addition, because of the manner in which the data are acquired and processed, the storage space required by both methods for achieving quadrature detection and obtaining spectra with pure-phase lineshapes (hypercomplex transform or TPPI) is twice that of the original method of achieving quadrature detection.

When faced with a structure elucidation problem, the choice between absolute-value and pure-phase modes of data presentation is determined by the acceptable level of compromise between final digital resolution in the 2D NMR spectrum and instrument measurement time. For high resolution, the pure-phase mode is chosen; conversely, for short measurement time, the absolute-value mode is chosen.

The pure-phase mode, in most cases, offers higher resolution since cross-peaks in this mode exhibit pure-absorption lineshapes. The antiphase character of individual cross-multiplets is useful in determining approximate values of coupling constants and in interpreting peaks within over-

lapped spectral regions. The advantages of the pure-phase mode are not without some penalty, however: high resolution requires long measurement times and storage of large data tables. More operator involvement is required due to the need to phase correct the 2D data. Additionally, in order to benefit most from zero filling and to avoid truncation artifacts, data should be sampled long enough to allow FIDs to decay fully, possibly further extending measurement time. When TPPI 2D NMR data are processed in the pure-phase mode and apodization functions are used, careful attention to their effect on 2D lineshapes is necessary so that artifacts in the final spectra are avoided, such as those arising from use of their sine-bell function (negative troughs at the base of peaks). Apodization functions that do not affect the beginning of the FID as drastically as the sine-bell function, such as the Lorentz/Gauss (40) and the shifted sine-bell (41) functions, can be used successfully when proper parameters are selected.

In contrast, the absolute-value mode is used when limited measurement time is available. The short measurement times result in low digital resolution; therefore, detailed information about coupling constants cannot be obtained and overlapped spectral regions are not well resolved. However, it is possible to identify coupling networks and assign less complicated spectra. The short measurement times will often result in truncated FIDs that necessitate the use of more drastic apodization functions, such as sine-bell or squared sine-bell, to minimize artifacts resulting from the truncated data. It is important to be aware that short measurement times may have the undesired effect of suppressing cross-peaks resulting from small J-coupling constants (7). If necessary, a delay can be inserted after each $\pi/2$ pulse to allow sufficient evolution for coherance transfer (t_1) or observation (t_2). Rapidly decaying apodization functions can also suppress this type of cross-peak.

To compare the absolute-value and pure-phase modes, spectra of 2 were obtained with TPPI and are shown in Fig. 8. The pure-phase spectrum (Fig. 8a) illustrates the delinea-

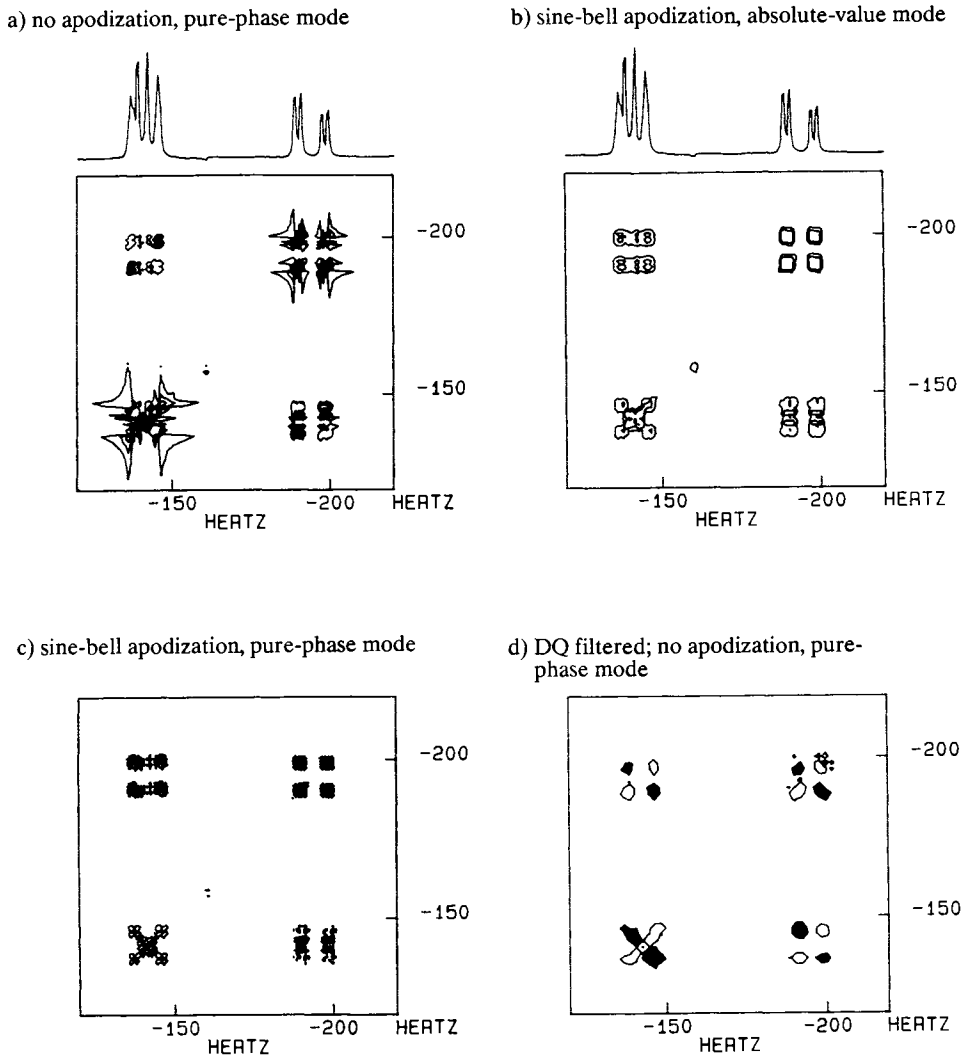

Fig. 8. COSY spectra of 5-bromoindole. TPPI acquisiton; 256 × 256 points, zero filled to 512 × 512. (a) No apodization, pure-phase mode; (b) sine-bell apodization in both dimensions, absolute-value mode; (c) sine-bell apodization in both dimensions, pure-phase mode; (d) DQ filtered, no apodization, pure-phase mode. The chemical-shift scale is the same as in Fig. 4.

tion between positive (open contours) and negative (filled contours) peaks that is characteristic of this mode. For comparison, in Fig. 8b a spectrum obtained by processing the same TPPI data in the absolute-value mode with sine-bell apodization is shown. Sine-bell apodization clearly removes the dispersive contributions (contours with pointed features) from the diagonal peaks. Shown in Fig. 8c is the spectrum in the pure-phase mode processed with sine-bell apodization to show the distortions (increased apparent multiplicity) that can be produced by the more drastic apodization functions in the pure-phase mode. When in doubt about whether to use the original method for quadrature detection in t_1 or TPPI, it is recommended that TPPI acquisition be used, since it is always possible to perform an absolute-value calculation on TPPI data, thus retaining the flexibility of presenting the data in either the pure-phase or the absolute-value mode. It should be remembered that TPPI acquisition will require twice the data storage space.

In contrast with single-pulse 1D NMR, in which all peaks can be phased to absorption, it is a general feature of 2D homonuclear correlation NMR that diagonal and cross-peaks are often of different phase (Table I), and it is not possible to phase cross-peaks and diagonal peaks simultaneously in absorption. Often, when the cross-peaks are phased to absorption, the diagonal peaks are left with dispersive character. Even though the cross-peaks in Fig. 8a are in pure absorption, the tails (the points on the diagonal contours) emanating from the dispersive diagonal peaks are clearly visible. Fortunately, relief from this complication can be obtained by adding what is known as a "double-quantum filter" (42) to the TPPI COBY experiment (Fig. 9).

Double-Quantum Filtered COSY

In a single-pulse 1D NMR experiment, only single-quantum (SQ) coherences exist. In a 2D NMR experiment such as COSY, however, the second pulse, when applied to a J-coupled spin system, creates additional orders of coherence, such as zero-quantum (ZQ), double-quantum (DQ), and higher-order coherences. It is only the SQ coherences existing after the second pulse that are detected in the COSY experiments described above, since non-SQ coherences cannot be observed directly (7).

The SQ coherences produce the undesirable diagonal-peak lineshapes in COSY described in the previous section. It was noted (42) that the invisible DQ coherences possess properties that would give desirable lineshapes. To observe these DQ coherences and simultaneously eliminate the SQ coherences, a phase-cycled $\pi/2$ pulse was added to the COSY experiment together with additional receiver phase cycling. These additions are called a DQ filter (actually a "DQ pass" filter), since, when four consecutive scans are coadded, the only signal remaining in the FID is that which existed as DQ coherence after the second pulse, the undesirable magnetizations being canceled ("filtered out"). The concept of the DQ filter can be understood clearly using the product operator formalism (19).

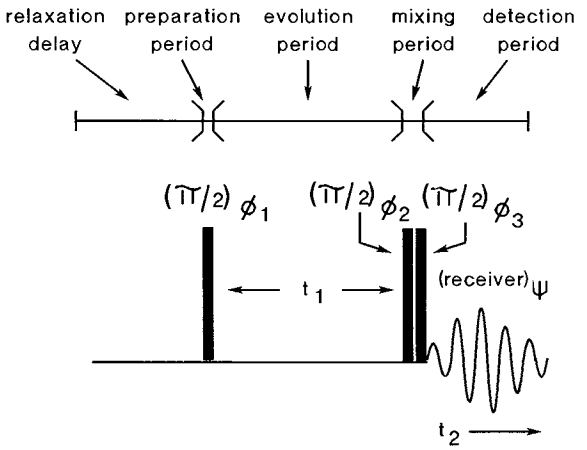

Fig. 9. Pulse sequence for double-quantum (DQ) filtered COSY.

The DQ filter consists of a pulse and receiver phase cycled in opposite directions. Intuitively, one might expect this counterrotation of pulse and receiver phases to cancel all signals after coaddition of four scans. This does, in fact, occur for the SQ signals on which our intuition has been developed, but the DQ coherences are twice as responsive to the 90° phase shifts and, hence, yield, after the pulse, observable single-quantum coherences that will coadd. They result in diagonal peaks and cross-peaks, both of which can be phased to absorption lineshape (absorptive antiphase; Table I), with no interfering dispersive tails from the diagonal peaks (Fig. 8d). The double-quantum filtered COSY experiment in the TPPI mode can be achieved with the following phase cycle.

	ϕ_1	ϕ_2	ϕ_3	ψ	
FID 1	x	x	x	x	Double-quantum filter
	x	x	y	$-y$	
	x	x	$-x$	$-x$	
	x	x	$-y$	y	
	y	y	y	y	CYCLOPS
	y	y	$-x$	x	
	y	y	$-y$	$-y$	
	y	y	x	$-x$	
	$-x$	$-x$	$-x$	$-x$	
	$-x$	$-x$	$-y$	y	
	$-x$	$-x$	x	x	
	$-x$	$-x$	y	$-y$	
	$-y$	$-y$	$-y$	$-y$	
	$-y$	$-y$	x	$-x$	
	$-y$	$-y$	y	y	
	$-y$	$-y$	$-x$	x	
FID 2	y	x	x	x	TPPI
	y	x	y	$-y$	
	.				
	.				
	.				
	etc.				

Scheme VIII

An additional benefit of the DQ filtered COSY experiment is the suppression of singlet resonances such as CH_3 peaks or solvent resonances; this results from the filtration process that removes SQ signals. The experiment suffers from a lower sensitivity than the normal COSY experiment [signal intensity is decreased by one-half (7)], but when high reso-

lution is desirable, we have found that the tradeoff of sensitivity for suppression of interfering dispersive diagonal resonances and other resonances such as singlets and solvent peaks is, as a general rule, very worthwhile.

ASSIGNMENT OF SPECTRA AND STRUCTURE ELUCIDATION

In this section are presented the most common 2D NMR techniques that are currently used to assign spectra and determine molecular structure. To make this Review of more general utility, most of the new methods are implemented on a spectrometer that does not have all the capabilities of the most current spectrometers but, however, does have capabilities that are most likely available on spectrometers purchased during the past 5 years. Ursolic acid (1), a triterpene of molecular weight 457, was chosen for purposes of illustration because it has a reasonably complex ^{1}H NMR spectrum and will demonstrate the utility of these techniques on a spectrum that cannot be assigned trivially.

In many cases it is not efficient to spend the time required to analyze completely a 2D NMR spectrum from one technique before applying another, since analysis of severly overlapped spectral regions can be very time-consuming. Often, analysis of data from subsequent methods can simplify the interpretation of previous data. Below we demonstrate this approach by applying the techniques in the order normally used in our laboratory. A detailed description of each resonance assignment is not given, but examples are presented to underscore the approach clearly.

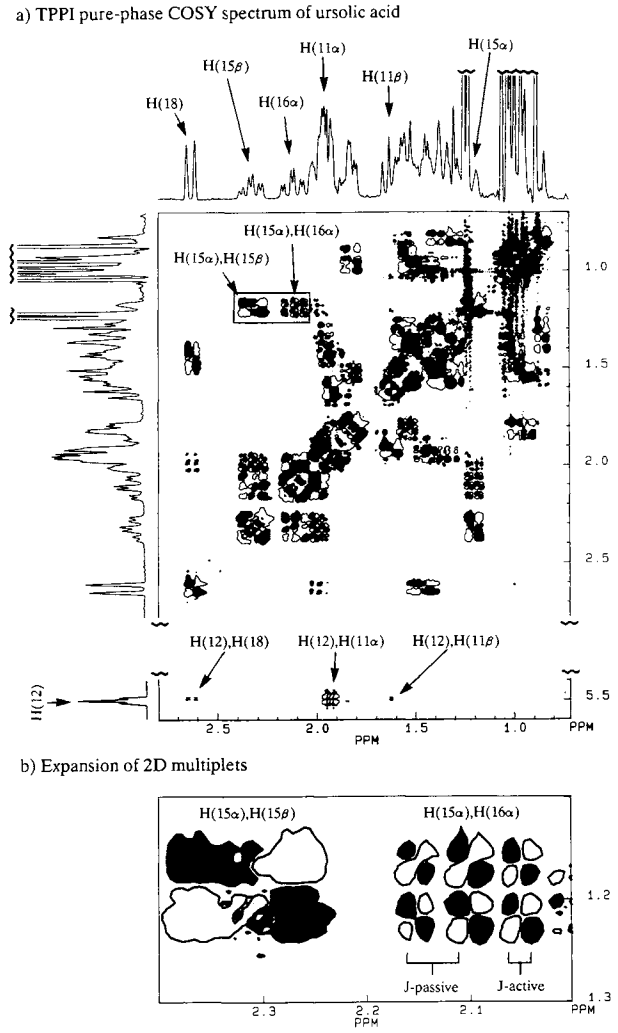

Fig. 10. DQ-filtered COSY spectrum of ursolic acid. TPPI acquisition; 800(t_1) × 1024(t_2) points, zero filled to 2048 × 2048; no apodization; pure-phase mode, both positive (open contours) and negative (filled contours) levels plotted. (a) Expansion of the spectral regions 0.7–2.8 and 5.4–5.6 ppm (ν_1)/0.7–2.8 ppm (ν_2); (b) expansion of the spectral region 1.1–1.3 ppm (ν_1)/2.0–2.4 ppm(ν_2).

COSY

In most cases, COSY provides the most structural information for a given amount of acquisition time. The DQ filtered COSY spectrum of **1** is shown in Fig. 10. The spectrum shown was acquired using TPPI and processed in the pure-phase mode, because it has been our experience that with complex spectra, we have benefited from the enhanced resolution of the pure-phase mode, and we have observed that the antiphase character of cross-multiplets has been very useful in assessing the approximate magnitudes of coupling constants. Shown also is the nomenclature that we use to identify these cross-multiplets. The peaks are labeled with the nuclei that correspond to the ν_1,ν_2 coordinates. Thus, the cross-multiplets indicated are labeled H(15α),H(15β) and H(15α),H(16α). The first represents chemical shift and coupling constant information of H(15α) evolving during t_1, transferred from H(15α) to H(15β) by the mixing pulse, and detected in H(15β) during t_2.

The approach in analyzing cross-peaks in the pure-phase DQ filtered COSY data in Fig. 10a is illustrated in Fig. 10b, in which is shown an expanded portion of the spectrum corresponding to the two cross-multiplets mentioned above. The 2D NMR resonance H(15α),H(16α) (equatorial,axial) consists of a six-peak by four-peak mutiplet. The H(15α), H(16α) coupling is responsible for the transfer of information between these two nuclei during the mixing pulse and is, therefore, referred to as the "active" coupling. This active coupling gives rise to the antiphase pairs of peaks within the cross-multiplets. The separation between these pairs therefore provides an estimate of the magnitude of this coupling. For the H(15α),H(16α) cross-multiplet, the coupling constant can be extracted from the 2D NMR resonance by simply starting at one corner of the square with one peak and moving in either direction until a peak of opposite sign is encountered. The remaining splittings result from oscillations of H(15α) that occurred during t_1 due to coupling with other nuclei and are known as "passive" couplings. In analyzing this resonance, starting in the lower right corner and moving left, one immediately encounters a peak opposite sign indicating that this ca. 4 Hz splitting is the active coupling between H(15α) and H(16α), consistent with their relative equatorial/axial orientation. This type of analysis must be approached with caution, however, since positive and negative peaks within complex multiplets often overlap, causing cancelation. For example, the H(15α),H(15β) reso-

Table II. ^1H and ^{13}C NMR Chemical Shifts[a] of Ursolic Acid

^1H	δ	^{13}C	δ
1α	0.95	1	39.1
1β	1.52		
2α	1.82	2	28.1
2β	1.82		
3	3.46	3	78.1
5	0.88	5	55.8
6α	1.56	6	18.8
6β	1.33		
7α	1.55	7	33.6
7β	1.35		
9	1.62	9	48.1
11α	1.94	11	23.6
11β	1.94		
12	5.50	12	125.7
15α	1.20	15	28.7
15β	2.33		
16α	2.12	16	24.9
16β	1.97		
18	2.62	18	53.6
19	1.45	19	39.5
20	0.93	20	39.4
21α	1.40	21	31.1
21β	1.40		
22α	1.95	22	37.5
22β	1.95		
23	1.23	23	28.8
24	1.01	24	16.5
25	0.87	25	15.7
26	1.04	26	17.5
27	1.21	27	23.9
29	0.98	29	17.5
30	0.93	30	21.4
		4	39.5[b]
		8	40.0
		10	37.3[b]
		13	139.3
		14	42.5
		17	48.1
		28	179.8

[a] As ppm relative to internal TMS.
[b] Assignments might be reversed.

nance should be a six-peak by four-peak cross-multiplet. However, the large geminal active coupling causes two peaks of opposite sign in the center of the multiplet's ν_2 dimension, resulting in partial cancelation; in the ν_1 dimension, the two pairs of peaks of the same sign on each side of the multiplet dimension are not resolved, producing a broad multiplet structure. As mentioned above, care must be taken with apodization functions applied to enhance resolution since they can produce artifacts that resemble peaks.

The assignment of a spectrum of this type usually begins with identification of one or more resonances that are isolated in chemical shift from other peaks in the spectrum and that have a ^1H chemical shift characteristic of a particular

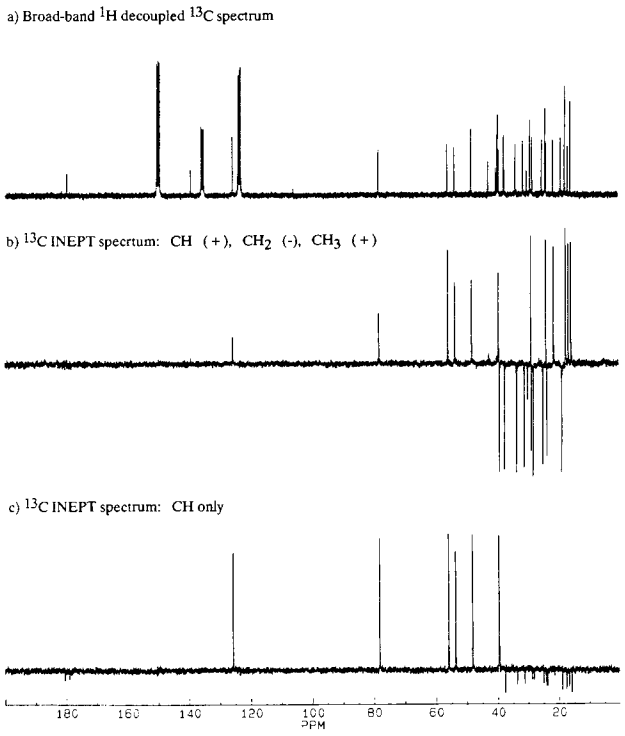

Fig. 11. ^{13}C NMR spectra of ursolic acid. (a) Broad-band ^1H decoupled spectrum; (b) INEPT spectrum with delays set to present CH_3 and CH resonances up (+) and CH_2 resonances down (−); (c) same as b except with delays set to present CH resonances only (+). Resonances at 124, 136, and 150 ppm in (a) are those of the solvent, pyridine-d_5.

chemical functionality. Thus, the lowest field peak at 5.50 ppm clearly corresponds to the olefinic H(12) (Fig. 10). By observing the cross-multiplet connectivities and splittings (as discussed in the previous paragraph) it is possible to identify ^1H peaks of hydrogens coupled to H(12) (Table II).

The procedure is repeated for all identifiable groups of peaks. Severe overlap of peaks often precludes a full assignment by one method. When the information supply from the

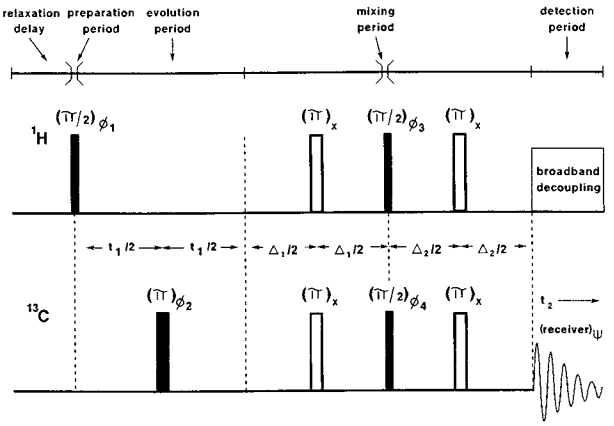

Fig. 12. Pulse sequence for ^{13}C-detected $^{13}C/^1H$ chemical shift correlation spectroscopy (CH COSY). Pulses indicated by open rectangles are used if pure-phase presentation is desired.

initial COSY analysis is exhausted, the next step in assignment usually involves 1D and 2D NMR ^{13}C–^{1}H heteronuclear experiments, provided that a sufficient quantity of sample is available to ensure that excessive instrument time will not be consumed by measurements of this type.

Heteronuclear Methods

One of the most generally useful methods for extracting structural information quickly from ^{13}C spectra is the 1D NMR method INEPT (Insensitive Nucleus Enhancement by Polarization Transfer) (43). This method is very convenient for determining carbon resonance type: CH_3, CH_2, CH, or quaternary C. DEPT (distortionless enhancement by polarization transfer) (44) provides an alternative approach for obtaining the same information. Neither of these methods is discussed here, but since the results are often critical for assignment of ^{13}C resonances and ultimately ^{1}H resonances, the normal and INEPT spectra of **1** are presented in Fig. 11.

2D Carbon Hydrogen Chemical-Shift Correlation NMR Spectroscopy

^{13}C-Detected CH COSY

Traditionally, the correlation of ^{13}C and ^{1}H chemical shifts has been accomplished by the pulse sequence shown in Fig. 12, in which the ^{13}C nuclei are detected during t_2 (^{13}C-detected CH COSY) (45,46). This choice of methodology was probably due to the configuration of existing spectrometers, on which this experiment could be implemented easily without extensive modifications. In the last few years, CH COSY is increasingly being achieved by techniques in which the more sensitive ^{1}H nuclei are detected (often referred to as "indirect detection") (47–51), thereby requiring a shorter measurement time. Since many laboratories still use the first method, we discuss both of these methods and compare them briefly.

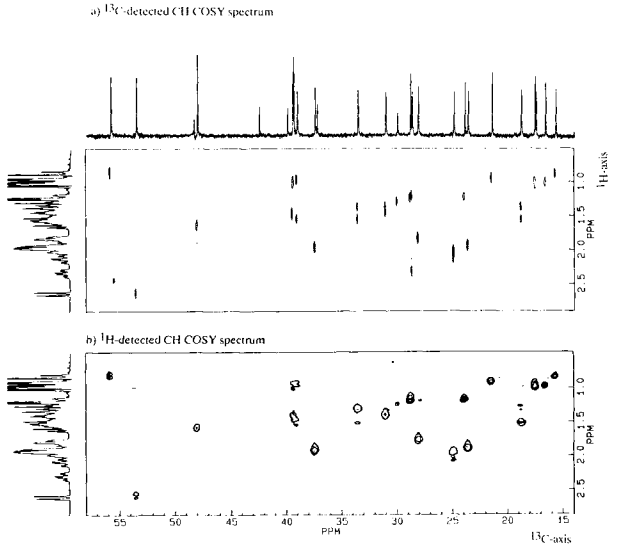

Fig. 13. (a) ^{13}C-detected CH COSY spectrum of ursolic acid. TPPI acquisition; 64 (t_1) × 2048 (t_2) points, zero filled to 128 × 2048; Gaussian/Lorentz apodization (t_1 and t_2); Δ_1 = 4 msec; Δ_2 = 3 msec; pure-phase mode, both positive and negative levels plotted. (b) ^{1}H-detected CH COSY spectrum (acquired using heteronuclear DQ coherence method). TPPI acquisition; 256 (t_1) × 2048 (t_2) points, zero filled to 512 × 2048; shifted (π/4) sine-bell apodization (t_1), 5-Hz exponential apodization (t_2); pure-phase mode, positive levels plotted; $1/(2J)$ = 4 msec, τ = 175 msec. For clarity, the ^{1}H-detected experiment is plotted with the ν_1 axis horizontal and the ν_2 axis vertical.

In ^{13}C-detected CH COSY, the preparation period consists of a ^{1}H $\pi/2$ pulse. During t_1, the chemical shift of each ^{1}H nucleus evolves. Although the ^{1}H doublet components (due to ^{1}H–^{13}C coupling) for each nucleus evolve also during t_1, the π ^{13}C pulse inserted in the middle of the evolution period inverts the carbon nuclei, causing the relative precession frequency of the doublet components to change sign, thereby refocusing them at the end of t_1. Therefore, there is no net evolution of the ^{1}H–^{13}C coupling during t_1, and the coupling does not appear as peak splitting in the ν_1 dimension; this is often referred to with the shorthand terminology "t_1 decoupling." Since the two doublet components are in phase at time t_1, no antiphase magnetization exists. As described earlier, the transfer of coherence during the mixing period relies on this antiphase magnetization. Consequently, a fixed delay Δ_1, usually set to $1/(2J)$ to ensure that the two coupling vectors are in complete antiphase, is inserted. The two simultaneous ^{1}H and ^{13}C $\pi/2$ mixing pulses transfer the ^{1}H NMR chemical shift evolution information to the corresponding ^{13}C nucleus.

^{13}C NMR spectra are usually acquired with ^{1}H broadband decoupling. If the decoupler were turned on immediately after the mixing pulses, no net signal would be detected, since antiphase ^{1}H magnetization produces antiphase ^{13}C magnetization during the mixing pulse. This type of magnetization has an equal number of spectral peaks up and down (see Fig. 5) and has no net integral; therefore, if the decoupler were turned on, no signal would be observed. This difficulty is alleviated by inserting a delay Δ_2 to allow the ^{13}C antiphase magnetization to evolve into in-phase magnetization. This delay is different in value from Δ_1 for the following reason. The ^{1}H spectrum containing ^{1}H–^{13}C coupling consists of doublets; in contrast, the ^{13}C spectrum containing ^{1}H–^{13}C coupling consists of doublets, triplets, and quartets, depending on the number of attached hydrogens. The antiphase signals corresponding to these different multiplicities refocus at different rates. To accommodate these different rates, a compromise value of $3/(8J)$ is chosen, thereby achieving an optimum balance of in-phase magnetization for all three situations.

In order to obtain pure-phase spectra, π pulses (indicated as open rectangles in Fig. 12) are inserted in the middle of Δ_1 and Δ_2 to refocus, respectively, the ^{1}H and ^{13}C chemical shifts, while allowing continued evolution due to J-coupling. These π pulses are technically not necessary, but without them, very large frequency-dependent phase corrections in both the ν_1 and the ν_2 dimensions would be required. Once the pulses have been included, the relationship between INEPT and this 2D method becomes clear. Pure-phase CH COSY spectra exhibit the same carbon-type delineation as do INEPT spectra. The following phase cycle is used for ^{13}C-detected CH COSY with TPPI.

	ϕ_1	ϕ_2	ϕ_3	ϕ_4	ψ				
FID 1	x	x	x	x	x	Axial peak elimination	π pulse imperfection elimination	CYCLOPS	TPPI
	x	x	$-x$	x	$-x$				
	x	$-x$	x	x	x				
	x	$-x$	$-x$	x	$-x$				
	x	x	x	y	y				
	x	x	$-x$	y	$-y$				
	x	$-x$	x	y	y				
	x	$-x$	$-x$	y	$-y$				
	x	x	x	$-x$	$-x$				
	x	x	$-x$	$-x$	x				
	x	$-x$	x	$-x$	$-x$				
	x	$-x$	$-x$	$-x$	x				
	x	x	x	$-y$	$-y$				
	x	x	$-x$	$-y$	y				
	x	$-x$	x	$-y$	$-y$				
	x	$-x$	$-x$	$-y$	y				
FID 2	y	x	x	x	x				
	y	x	$-x$	x	$-x$				
	y	$-x$	x	x	x				
	y	$-x$	$-x$	x	$-x$				
				etc.					

Scheme IX

In addition to participating in the coherence transfer, the final $\pi/2$ carbon pulse generates in-phase ^{13}C magnetization from the longitudinal ^{13}C z magnetization existing at the time of the pulse, which, if not suppressed, would result in axial peaks. Altering the phase of the final ^1H pulse $(x, -x)$ changes by 180° the phase of the ^{13}C antiphase magnetization, whereas the ^{13}C in-phase magnetization remains unaffected. Therefore, if, as indicated in the phase cycle, the receiver phase is alternated in concert with the ^1H pulse, the desired antiphase signals will coadd, and the ^{13}C in-phase signals will cancel.

Alternating the phase of the first ^{13}C π pulse by 180° $(x, -x)$ cancels artifacts due to imperfections in that pulse. If it is necessary to suppress artifacts resulting from imperfections in the π pulses indicated by the open rectangles, these pulses may be phase cycled independently from the other pulses (this, however, increases the experiment time considerably). The spectrum shown in Fig. 13 was obtained with constant phase (x) of these pulses. CYCLOPS is achieved by incrementing the final carbon pulse phase and receiver phase together.

The ^{13}C-detected CH COSY spectrum of 2 is shown in Fig. 13 [not shown are the low-field ^1H and ^{13}C NMR peaks of H(12) and H(3) since their assignment is obvious from their chemical shifts]. Δ_1 is set to a value of 4 msec ($1/2J_{ave.}$ = $1/[2 \times 125\ Hz]$ = 4 msec) to ensure that cross-peaks result from scalar coupling between the directly bonded ^1H's and ^{13}C's. (Δ_1 and Δ_2 can, however, be adjusted to select for smaller long-range couplings to identify, for example, quaternary carbons (4).) Carbon types are delineated in the same manner as INEPT: CH_3 positive (open contours), CH_2 negative (filled contours), and CH positive. Although a high-digital resolution INEPT spectrum can be used to advantage to assign carbon types in cases where 2D cross-peaks are closely spaced, the phase-sensitive CH COSY spectrum provides this same information.

Other approaches to obtaining pure-phase ^{13}C-detected CH COSY spectra exist. For example, an approach based on DEPT (44,52) uses fewer rf pulses, provides similar results, and can be used to advantage in studying molecules with a wide range of ^{13}C-^1H coupling constants. This method involves heteronuclear multiple-quantum coherence and is similar in concept to ^1H-detected CH COSY discussed below.

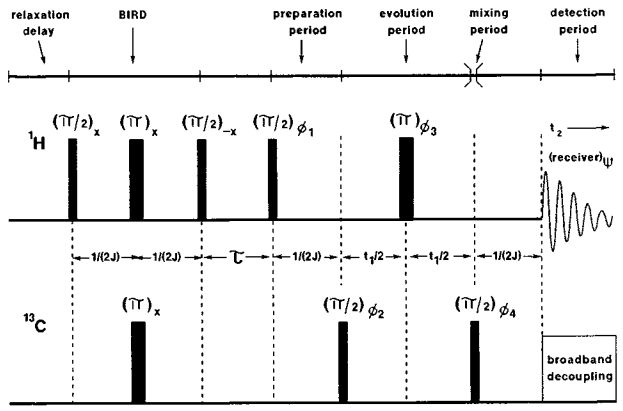

Fig. 14. Pulse sequence for ^1H-detected CH COSY (heteronuclear DQ coherence method) with BIRD composite pulse for suppression of $^1H^{12}C$ signals.

^1H-Detected CH COSY

In the other principal approach to obtaining CH COSY spectra, the more sensitive ^1H nuclei are detected as originally suggested by Bodenhausen and Ruben (53). This approach has the immediate appeal of offering shorter data acquisition times but is considerably more difficult from an experimental standpoint. The ^1H signals that are detected are those corresponding to hydrogens bonded to ^{13}C atoms. Those bonded to the 99 times-more-abundant ^{12}C atoms produce a large signal that must be suppressed to overcome the dynamic range limitation of analog-to-digital converters. In addition, the complete ^{13}C chemical shift range must be irradiated to achieve decoupling during t_2. Fortunately, pulse sequences have been designed to suppress the unwanted $^1H^{12}C$ signals (54,55), and composite pulse decoupling methods (56–59) provide very efficient ^{13}C decoupling over wide chemical shift ranges. The principal limitation remains that most existing spectrometers cannot perform these experiments without modification, in most cases, by the manufacturer.

Several approaches have been used for ^1H-detected CH COSY (48,60–63). The pulse sequence in Fig. 14 illustrates an approach that is more commonly used, based on heteronuclear multiple quantum coherence (47). Before the actual pulse sequence begins with the preparation period, a group of pulses and delays referred to as a "BIRD composite pulse" (54,55) is inserted to aid in suppressing the intense $^1H^{12}C$ signal. (The BIRD composite pulse is technically not essential because the $^1H^{12}C$ signal can be removed by phase cycling and subtraction of successive scans; however, the full signal would need to be digitized, placing severe dynamic range demands on the digitizer.) After the last $\pi/2$ pulse of the composite pulse, magnetization from non-

^{13}C-coupled hydrogens is aligned along $-z$ in the rotating frame, and magnetization from ^{13}C-coupled hydrogens is aligned along $+z$. The delay τ allows the magnetization along $-z$ to begin returning to equilibrium due to spin-lattice relaxation. As this magnetization passes through zero, the preparation period is begun with a ^{1}H $\pi/2$ pulse.

Since ideally the non-^{13}C-coupled hydrogen magnetization has a value of zero at this time, the only in-plane magnetization generated by the pulse is that due to ^{13}C-coupled hydrogens. The delay of $1/(2J)$ allows the ^{1}H magnetization to evolve from in-phase fully into antiphase. At this time, a $\pi/2$ pulse is applied to the ^{13}C nuclei. This pulse converts the antiphase ^{1}H magnetization fully into heteronuclear two-spin coherence (in this case, a combination of ZQ and DQ coherence). During t_1, two-spin coherence evolves. Although two-spin coherence evolves at either the sum (double quantum) or the difference (zero quantum) of the chemical shifts of the two coupled nuclei, it is possible, by use of a π pulse, to refocus the chemical shift contribution of one nucleus to this evolution. The ^{1}H π pulse in the middle of t_1 causes the ^{1}H chemical shift part of the two-spin coherence to refocus, whereas the ^{13}C chemical shift part continues to evolve. Effectively, therefore, only ^{13}C chemical shift evolves during t_1. The final ^{13}C $\pi/2$ pulse converts the two-spin coherence back into antiphase ^{1}H coherence whose amplitude has been modulated by ^{13}C chemical shift. During the final $1/(2J)$ delay, this antiphase magnetization evolves into in-phase ^{1}H magnetization that can then be decoupled from the ^{13}C nuclei. The symmetrical placement of the $1/(2J)$ and $t_1/2$ periods on both sides of the final ^{1}H π pulse ensures that no ^{1}H chemical shift evolution occurs between the first preparation pulse and the detection period. This simplifies considerably phase correction in the ν_2 dimension of the 2D spectrum. Since ^{1}H-^{1}H homonuclear coupling is not refocussed in this pulse sequence, spectra obtained at high digital resolution will contain peaks with antiphase character. The following phase cycle is used for ^{1}H-detected CH COSY with TPPI.

	ϕ_1	ϕ_2	ϕ_3	ϕ_4	ψ		
FID 1	x	x	x	x	x	Suppress $^1H^{12}C$ signal	
	x	x	x	$-x$	$-x$		
	x	$-x$	x	x	$-x$		
	x	$-x$	x	$-x$	x		
FID 2	x	y	x	x	x	TPPI	
	x	y	x	$-x$	$-x$		
	x	$-y$	x	x	$-x$		
	x	$-y$	x	$-x$	x		
	.						
	.						
	etc.						

Scheme X

TPPI is accomplished by incrementing the phase of the first ^{13}C pulse (ϕ_2) by 90° on successive FIDs. Since all ^{1}H nuclei do not have the same relaxation rate, the value of τ chosen must be a compromise. Therefore, residual signals due to ^{12}C bound hydrogens may exist during detection. To alleviate this difficulty, the phases of both ^{13}C $\pi/2$ pulses are alternated independently by 180° within each FID together with the receiver. (In fact, phase alternation of only one of either of these two ^{13}C pulses is required.) This suppresses any residual signal due to $^1H^{12}$C magnetization not fully removed by the BIRD composite pulse and delay τ. Alternation of the phases of these pulses does not affect the residual $^1H^{12}$C signal but reverses the phase of the desired signal, so that the receiver phase alternation removes the undesired signal.

It has been observed empirically (64) that minimum phase cycling produces the best results in this experiment, so that no ^{1}H phase cycling is used. The necessity for minimum phase cycling is likely due to the fact that full relaxation of nuclei does not normally occur during the relaxation delay between scans; the minimum phase cycle should allow a closer approach to a consistent steady-state condition to keep the very large undesirable $^1H^{12}$C signal from producing artifacts.

During acquisition, ^{13}C decoupling must be applied to remove the ^{1}H–^{13}C coupling. To cover the wide chemical-shift range and simultaneously minimize decoupler power, a composite pulse ^{13}C sequence known as GARP (59) was used. Other composite sequences, such as MLEV-16 (56) and WALTZ-16 (57,58), have been used also with equally good results.

The choice between ^{13}C- and ^{1}H-detected CH COSY involves several considerations. Of course, without the requisite hardware centered around observing ^{1}H and decoupling ^{13}C, only ^{13}C detection can be accomplished. In those cases in which large amounts of sample are available and low solubility is not a problem, ^{13}C detection is more straightforward to set up experimentally. In addition, more often than not, with this method, fewer FIDs are required in the t_1 dimension to achieve a given hertz per point resolution, since the ^{1}H sweep width is usually about one-fifth that of the ^{13}C sweep width.

It is often the case, however, that only small amounts of sample are available, and the number of ^{13}C scans required for good S/N exceeds significantly the minimum phase cycle length. In this case, the high γ (magnetogyric ratio) of ^{1}H makes ^{1}H-detected CH COSY the method of choice. For many samples, only two or four scans are required for each t_1 value, and even though a large number of t_1 FIDs must be acquired to achieve a desired ^{13}C resolution, the high S/N makes the ^{1}H-detected experiment very attractive.

There are three principle factors that determine the relative sensitivity of ^{1}H and ^{13}C-detected CH COSY experiments (7). (i) The nucleus excited in the preparation period produces magnetization that is carried through the various coherences in the pulse sequence to be detected during t_2; if ^{1}H is excited instead of ^{13}C, there is an approximately fourfold sensitivity advantage due to the more favorable ^{1}H Boltzmann distribution ($\gamma_H/\gamma_C \simeq 4$). (ii) The response observed during the detection period is proportional to γ^2 of the

Table III. The Relative Sensitivity of CH COSY Experiments

Preparation	Evolution	Detection	Relative Sensitivity
^{1}H	^{13}C	^{13}C	1 (Fig. 12)
^{13}C	^{13}C	^{1}H	2
^{1}H	DQ, ZQ	^{1}H	8 (Fig. 14)

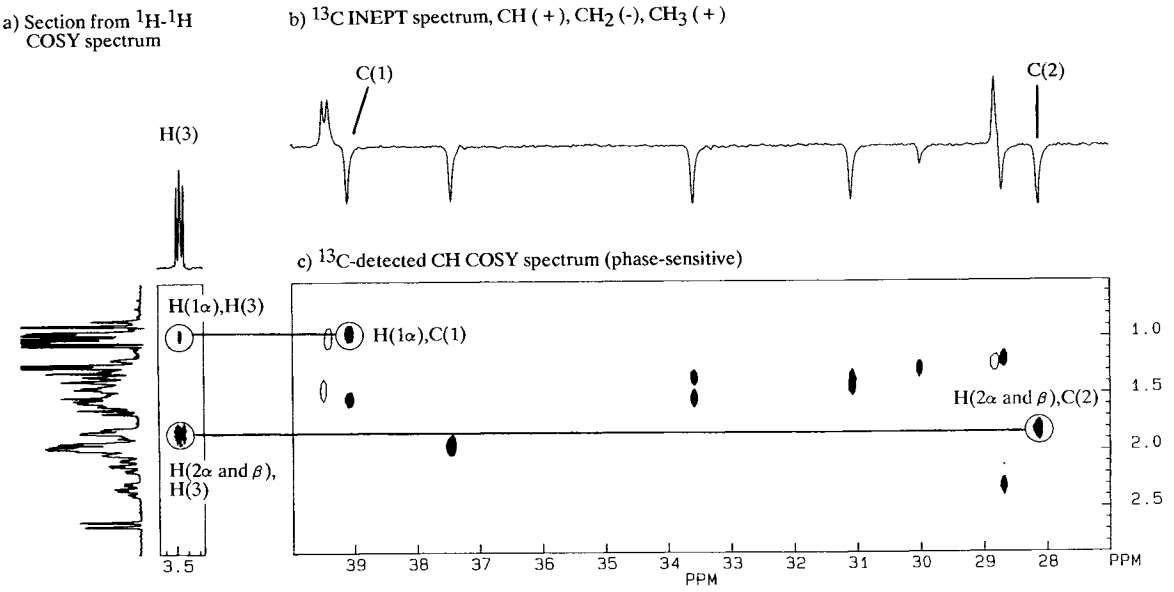

Fig. 15. The use of pure-phase CH COSY spectrum for assignment of ^{13}C and ^{1}H resonances of positions 1–3 of ursolic acid. (a) Expansion of ^{1}H COSY spectrum of ursolic acid, spectral region 0.5–2.9 ppm (ν_1)/3.3–3.6 ppm (ν_2); (b) ^{13}C INEPT spectrum for region 27.0–40.0 ppm with delays set to present CH_3 and CH resonances up (+) and CH_2 resonances down (−); (c) pure-phase ^{13}C- detected CH COSY spectrum, spectral region 0.5–2.9 ppm (ν_1)/27.0–40.0 ppm (ν_2), with delays set to present CH_3 and CH resonances up (+; open contours) and CH_2 resonances down (−; filled contours).

nucleus observed, and the noise of the receiver is observed empirically to be proportional to $\gamma^{1/2}$, giving S/N $\propto \gamma^{3/2}$; this results in an increase in sensitivity of 8 [$(\gamma_H/\gamma_C)^{3/2} = 8$] for detection of ^{1}H over ^{13}C. (iii) The spin-lattice relaxation time (T_1) of the nucleus excited during the preparation period determines the maximum rate at which the pulse sequence can be repeated; since, in general, ^{1}H nuclei have shorter T_1's than ^{13}C nuclei, it is advantageous to excite ^{1}H during the preparation period. Because of factors i and iii, the two CH COSY methods presented in the Review begin with ^{1}H magnetization.

Table III outlines the relative sensitivity of the more commonly used CH COSY experiments (7), neglecting relaxation time effects (factor iii above). Since there are additional instrumental and spectral factors that influence sensitivity, these values should be viewed only as estimates. For comparison purposes, the sensitivity is presented of ^{1}H-detected methods in which ^{13}C magnetization is excited during the preparation period. The ^{1}H-detected CH COSY and ^{13}C-detected CH COSY spectra of **1** are presented in Fig. 13. The ^{1}H-detected spectrum shown was obtained using a standard ^{13}C probe with observation over the ^{1}H decoupler coil; therefore, it was not obtained under ideal sensitivity or lineshape conditions. Using a probe designed for ^{1}H observe and ^{13}C decoupling, better results would be obtained.

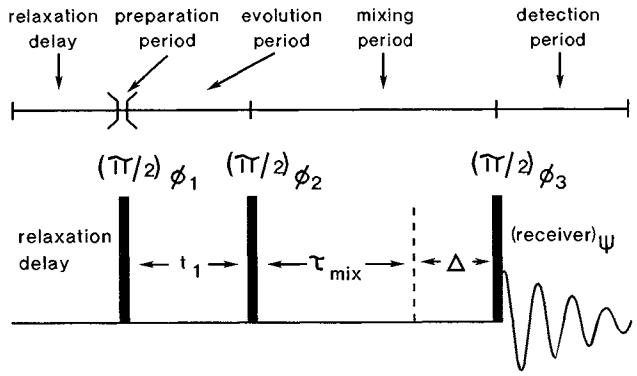

Fig. 16. Pulse sequence for 2D NOE correlation spectroscopy (NOESY).

Once the INEPT and CH COSY spectra have been obtained, the process of assignment can continue, including cross-checking and updating assignments by referring simultaneously to the COSY and CH COSY spectra. During this process, it is possible to eliminate ambiguities that appear during the initial COSY analysis. For example, H(3) exhibits two COSY cross-peaks (Fig. 10), one at 1.82 ppm and one at 0.95 ppm. One might expect these two peaks to correspond to coupling with H(2α) and H(2β). However, in the CH COSY spectrum (Fig. 15), the $C(2)H_2$ resonance displays only one cross-peak, at 1.82 ppm. This indicates that both $H(2\alpha)$ and $H(2\beta)$ resonate at 1.82 ppm. The other COSY cross-peak at 0.95 ppm (Fig. 10) has been identified as being due to long-range coupling between H(3) and H(1α). The cross-comparison of COSY and CH COSY spectra is pursued until no further assignments can be obtained.

2D Nuclear Overhauser Effect Spectroscopy (NOESY)

Traditionally, 1D NMR structure elucidation methods that delineate the covalent structure of molecules by using coupling constants have been supplemented by methods that measure through-space proximity of nuclei via the nuclear Overhauser effect (NOE). In 2D NMR, COSY and CH COSY are supplemented by NOESY (17). The intereaction that is detected in NOESY is cross-relaxation due to dipolar

coupling between nuclei that are in proximity (65). In cross-relaxation, two dipolar-coupled nuclei flip simultaneously, altering their individual contributions to their respective z components of magnetization.

In NOESY (pulse sequence in Fig. 16), the nuclei are prepared by a $\pi/2$ pulse, after which chemical shift and coupling evolve during t_1. The second $\pi/2$ pulse samples the in-phase magnetization, placing a part of it back along the z axis. During the mixing period τ_{mix}, the z components of dipolar coupled nuclei interchange partially due to cross-relaxation. Since the in-phase magnetization of a given nucleus is precessing during t_1, the magnitude returned to the z axis by the second pulse will be modulated by the chemical shift of that nucleus. Therefore, the extent of internuclear z component interchange will be modulated by the chemical shifts, so that after the mixing period, the z components of nuclei will carry chemical-shift information of nuclei to which they are diploar coupled. These modulated z components are sampled by the third $\pi/2$ pulse. The resulting FIDs therefore contain signals that, upon 2D Fourier transformation, produce cross-peaks that are diagnostic of internuclear dipolar coupling and, therefore, spatial proximity.

As one might expect from the previous COSY discussion, the second $\pi/2$ pulse in the NOESY pulse sequence also serves to transfer antiphase coherence between spin-coupled nuclei. This is undesirable in NOESY since this coherence transfer, if not suppressed, will lead to extra cross-peaks that are not directly related to through-space proximity. Phase cycling is used to eliminate residual single-quantum signals that exist during τ_{mix}. The second pulse also generates ZQ and DQ coherences that may produce interfering signals when sampled by the third pulse (66). All SQ and DQ coherences are eliminated by the following phase cycle (24), which also permits TPPI acquisition.

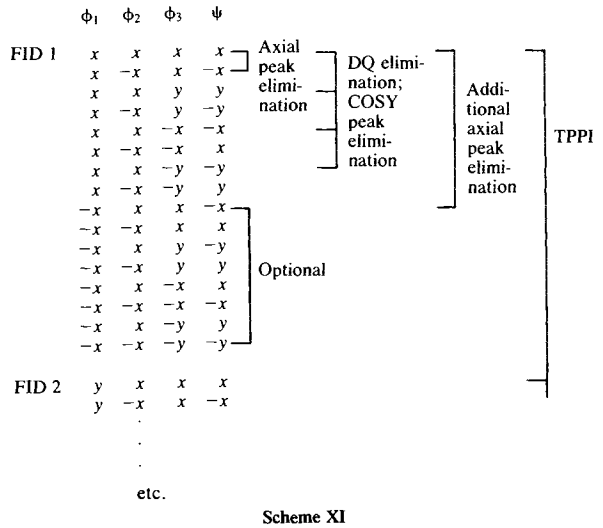

Scheme XI

Artifacts due to the presence of ZQ coherences in NOESY cannot be removed by phase cycling but can be eliminated by adding a small random-length delay Δ to the mixing period (66). For each random-length delay, an additional 16 scans must be obtained. The random delay must not be varied during the 16-scan phase cycle or the purpose of the phase cycle will be defeated, and artifacts due to SQ and DQ coherence will not subtract properly during coaddition of the 16 scans. The random delay Δ should be in the range 0.0 sec to $1/(\nu_A - \nu_B)$, where A and B are the two coupled nuclei exhibiting the smallest chemical shift difference in the spectrum (e.g., 0–20 msec for nuclei 50 Hz apart). This will allow the ZQ coherence, which evolves at a rate equal to the difference in chemical shift of the two nuclei involved, to be randomized on coaddition of several sets of 16 scans within one t_1 value. The same set of Δ values should be used for all t_1 values. If the total number of scans for each t_1 value becomes excessive, the minimum phase cycle can be reduced to eight, as indicated. Artifacts due to ZQ coherences can also be suppressed significantly by using a constant τ_{mix} with a randomly or systematically placed π pulse within the mixing period (66). An alternate method for eliminating artifacts due to all orders of coherence involves the use of a homogeneity-spoiling pulse inserted at the beginning of the mixing period; experimentally, however, this can be more problematic, since it can produce field/frequency lock instability.

The TPPI NOESY spectrum of **1** is shown in Fig. 17. It illustrates the assignment of hydrogens proximal to H(3), e.g., *H*(1α) referred to in the section above. There is a cross-peak *H*(1α),*H*(3) at 0.95, 3.46 ppm, the same position at which a cross-peak appeared in the DQ filtered COSY spectrum. This cross-peak results from dipolar interaction between these nuclei that are in proximity due to their 1,3 diaxial orientation in the same ring. In addition, cross-peaks are also observed in this ν_2 column for H(2α), C*H*$_3$(24), and H(5), nuclei that are also in proximity. The complementary nature of COSY and NOESY data allows further assignments to be made and others confirmed.

As the molecular weight increases (≳1000), the magnitude of the ^{1}H–^{1}H NOE becomes increasingly smaller (65). This is a result of the slower tumbling motion of larger molecules. As the tumbling correlation time approaches the reciprocal of the spectrometer frequency ($\tau_c\omega_o \simeq 1$), the NOE decreases from a maximum of 50% to approach 0% and becomes negative, reaching a maximum negative value of −100% for very large molecules (67). In addition, for very large molecules, spin diffusion reduces the specificity of the NOE measurement (68). These factors place limitations on the NOESY experiment for applications to macromolecules. For a given molecular weight, the NOE also decreases with increasing magnetic field. To circumvent the problem of very small NOEs, an experiment known both as CAMELSPIN (67) and ROESY (Rotating frame nuclear Overhauser Effect SpectroscopY) (69) was developed.

Whereas NOESY measures the extent of z-component interchange during the mixing period, the rotating frame experiment monitors the extent of x-component (or y-component) interchange under the influence of a "spin-lock" (see below) during the mixing period. The rotating frame nuclear Overhauser effect is always positive, increasing from ~40% for small molecules to ~70% for very large molecules (67), thereby overcoming a limitation to the NOESY experiment. CAMELSPIN or ROESY requires extremely careful control of experimental conditions, as well as very cautious interpretation of data, since cross-peaks can be present in the final 2D spectrum that do not necessarily reflect rotating frame cross-relaxation. Much effort has gone

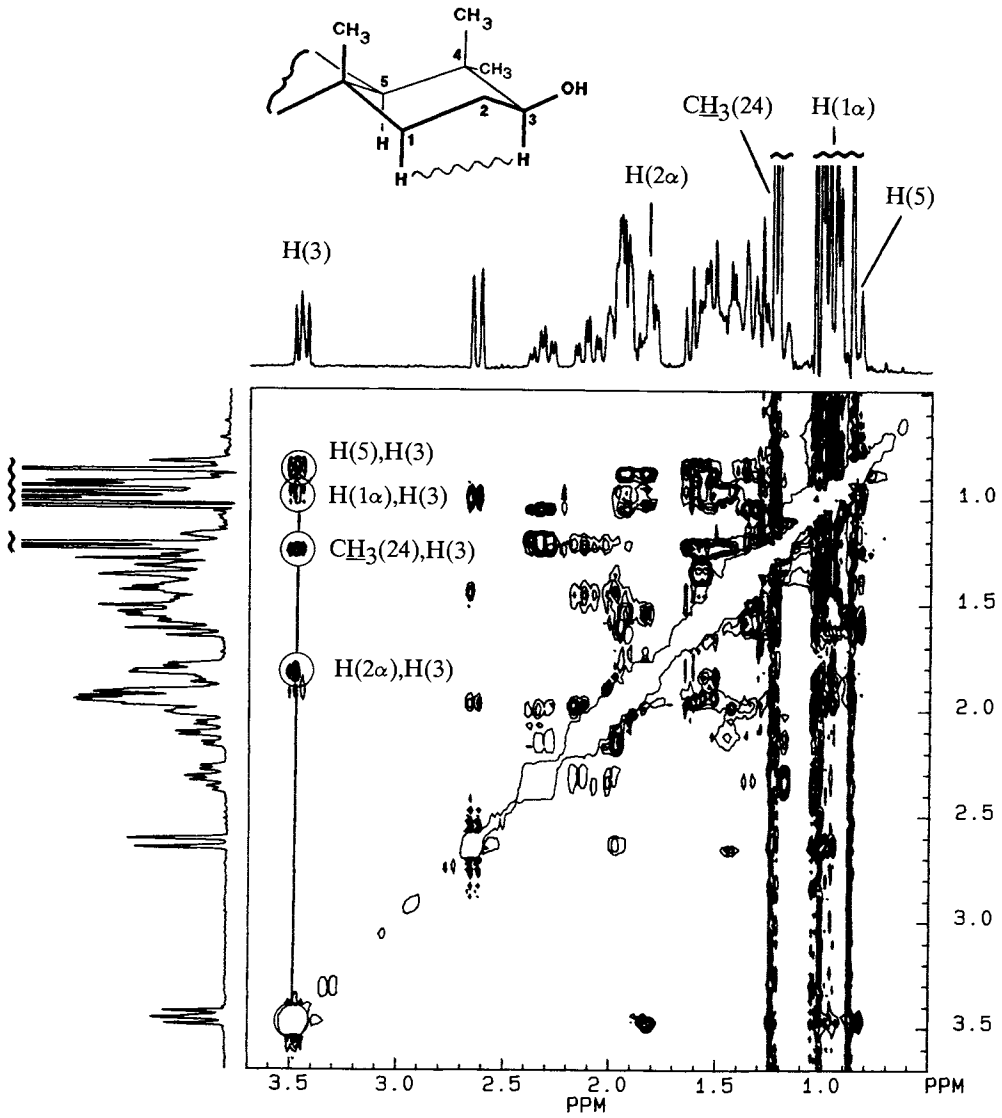

Fig. 17. NOESY spectrum of ursolic acid. TPPI acquisition; 512 (t_1) × 4096 (t_2) points, zero filled to 1024 × 4096; Lorentz/Gauss apodization (both t_1 and t_2); pure-phase mode, only negative levels plotted; τ_{mix} = 240 msec; eight different values of Δ used, randomly chosen between 0 and 20 msec. Expansion of spectral region (0.5–3.7 ppm (ν_1)/0.5–3.7 ppm (ν_2). Assignments of hydrogens spatially proximal to H(3) are illustrated.

into methodology for eliminating or distinguishing these contaminating peaks (69–71). Although the rotating frame cross-relaxation experiment has proven itself invaluable in studies of intermediate-sized molecules, we do not present data from this experiment in this review, since the NOESY experiment provides the necessary information for analyzing 1, with fewer potentially misleading artifacts.

Specialized Experiments

COSY allows the elucidation of molecular structure by exploiting interactions that occur through generally two or three bonds. Often, however, it is helpful to employ techniques that probe the framework of a molecule over larger numbers of bonds. Although, in some respects, NOESY supplies this type of information, it relies on through-space interactions and, therefore, may not reveal the bonding skeleton of a molecule. Several methods that have proven especially useful exploit interactions occurring over several bonds. Here we discuss two of these.

Relayed COSY

COSY is limited to examining nuclei that are directly J-coupled. An extension of COSY, relayed COSY (72–75), is used to observe nuclei that, although not directly coupled to one another, are both coupled to a third nucleus. This nucleus serves as a "relay" to allow communication between the two noncoupled nuclei.

The pulse sequence for relayed COSY is shown in Fig. 18. For illustration, consider a spin system AMX, in which nuclei A and X are coupled to M but not to each other ($J_{AM}, J_{MX} \neq 0$; $J_{AX} = 0$). Using nucleus A as an example, the first $\pi/2$ pulse creates in-phase A magnetization, which

evolves during t_1 into antiphase A magnetization. This is referred to as "A magnetization antiphase with respect to M," because it is the coupling J_{AM} that causes the two A magnetization vectors to "fan out."

$$\text{In-phase}_A \xrightarrow{J_{AM}} \text{Antiphase}_A \quad \text{(with respect to M)}$$

The second $\pi/2$ pulse converts antiphase A magnetization (with respect to M) into antiphase M magnetization (with respect to A), transferring A chemical-shift information to M.

$$\text{Antiphase}_A \text{ (with respect to M)} \xrightarrow{\pi/2}$$
$$\text{Antiphase}_M \text{ (with respect to A)}$$

So far, the method is identical to COSY. However, during the mixing period τ, as antiphase M magnetization (with respect to A) is converted into in-phase M magnetization, a simultaneous conversion occurs of this in-phase M magnetization into a different type of antiphase M magnetization (with respect to X), reflecting the interaction between M and X. The net effect is summarized as follows.

$$\text{Antiphase}_M \text{ (with respect to A)} \xrightarrow{J_{AM},J_{MX}}$$
$$\text{Antiphase}_M \text{ (with respect to X)}$$

The third $\pi/2$ pulse produces the desired antiphase X magnetization.

$$\text{Antiphase}_M \text{ (with respect to X)} \xrightarrow{\pi/2}$$
$$\text{Antiphase}_X \text{ (with respect to M)}$$

This antiphase X magnetization then evolves into observable in-phase magnetization that carries A chemical-shift information via the relay process through M. Therefore, the 2D NMR spectrum contains off-diagonal peaks between A and X. In addition to the relayed COSY cross-peaks, it is a complication of this experiment that normal COSY peaks are also observed (75). The π pulse in the middle of τ refocuses chemical shift to allow pure-phase presentation of the 2D NMR spectra. The following pulse sequence is used to produce relayed COSY spectra with TPPI.

	ϕ_1	ϕ_2	ϕ_3	ϕ_4	ψ	
FID 1	x	x	x	x	x	Axial t_1 peak elimination; DQ elimination; Axial τ peak elimination
	x	$-x$	x	x	x	
	x	x	x	$-x$	x	
	x	$-x$	x	$-x$	x	
	y	y	y	y	y	CYCLOPS
	y	$-y$	y	y	y	
	y	y	y	$-y$	y	
	y	$-y$	y	$-y$	y	
	$-x$	$-x$	x	$-x$	$-x$	
	$-x$	x	x	$-x$	$-x$	
	$-x$	$-x$	x	x	$-x$	
	$-x$	x	x	x	$-x$	
	$-y$	$-y$	y	$-y$	$-y$	
	$-y$	y	y	$-y$	$-y$	
	$-y$	$-y$	y	y	$-y$	
	$-y$	y	y	y	$-y$	
FID 2	y	x	x	x	x	TPPI
	y	$-x$	x	x	x	
	y	x	x	$-x$	x	
	y	$-x$	x	$-x$	x	
	.					
	.					
	etc.					

Scheme XII

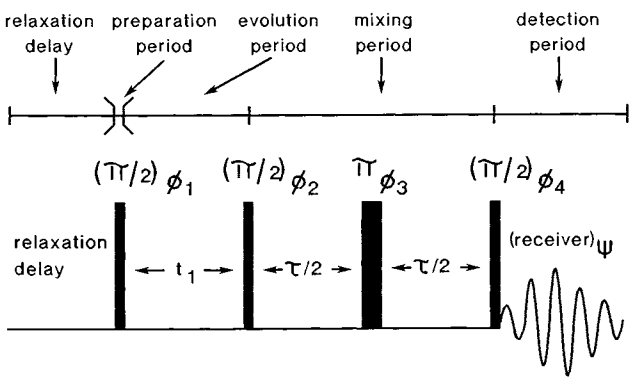

Fig. 18. Pulse sequence for 2D relayed coherence transfer correlation spectroscopy (relayed COSY).

Phase cycling of the second pulse eliminates axial peaks due to z magnetization that returns during t_1 and simultaneously selects against DQ coherences that might produce interfering signals during t_2. Phase cycling of the third pulse eliminates axial peaks due to z magnetization returning during τ.

The relayed COSY spectrum of 1 is shown in Fig. 19. Highlighted are the cross-peaks that are observed for H(18). The cross-peaks H(16β),H(18) and H(19),H(18) are COSY peaks and result from coherence transferred to H(18) by the second $\pi/2$ pulse (compare with the COSY spectrum in Fig. 10). The relay cross-peak H(15β),H(18) results from coherence transferred from H(15β) to H(16β) by the second pulse and then relayed from H(16β) to H(18) by the fourth pulse. The origin of cross-peak H(20),H(18) can be traced similarly. As can be seen, the relay cross-peaks and COSY cross-peaks can be easily distinguished by comparing the COSY and relayed COSY spectra, since the relay cross-peaks usually do not appear in the COSY spectrum. In principle, it is

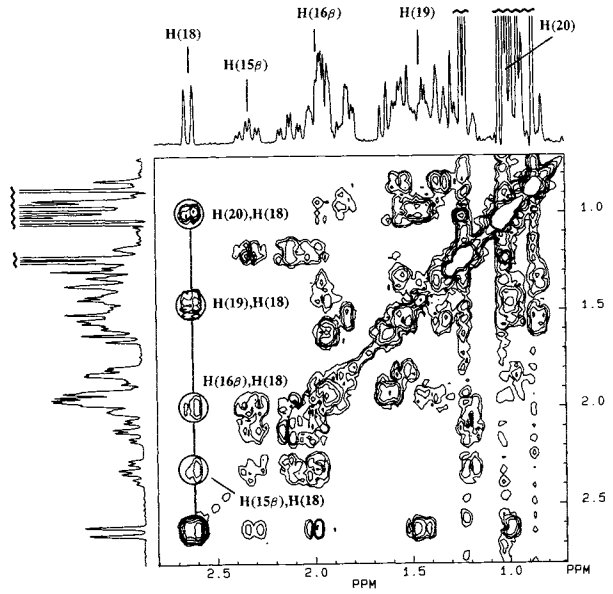

Fig. 19. Relayed COSY spectrum of ursolic acid. TPPI acquisition; 512 (t_1) × 1024 (t_2) points, zero filled to 1024 × 1024; squared sine-bell apodization (both t_1 and t_2); data plotted in magnitude mode; τ = 70 msec. Expansion of spectral region 0.7–2.8 ppm (ν_1)/0.7–2.8 ppm (ν_2). Assignments of hydrogens remote to H(18) are illustrated.

also possible in the pure-phase spectrum to distinguish between relay and COSY cross-peaks, since the relay peaks appear in absorptive antiphase and the COSY peaks are a mixture of absorptive and dispersive components (75–77) (Table I). However, the spectrum shown is an absolute-value presentation of TPPI-acquired data; this was required since sine-bell apodization was used to suppress very large diagonal tails from CH_3 singlets, as well as interferences from the dispersive components of COSY peaks. As with COSY, a DQ filtered (actally double-DQ filtered) version of relayed COSY exists (76,77) to minimize interference from diagonal tails and to eliminate the dispersive contributions to COSY peaks, thereby allowing both COSY and relayed COSY peaks to appear in absorptive antiphase. The sensitivity of this method, however, is lower by a factor of 4.

Experiments Utilizing In-Phase Coherence Transfer

All of the experiments discussed so far, except NOESY (and ROESY), require coherence transfer involving antiphase magnetization. Under the influence of a spin-lock, it is possible to achieve coherence transfer of in-phase magnetization between J-coupled nuclei. This has led to an extremely useful group of experiments, TOCSY (TOtal Correlation SpectroscopY) (78) or HOHAHA (HOmonuclear HArtmann–HAhn spectroscopy) (79,80), that allow examination of extended networks of nuclei in a "relay" sense. Using these methods, it is possible to delineate groups of nuclei in which each nucleus is coupled to at least one other member of the group. TOCSY or HOHAHA can be particularly useful in isolating subspectra of subunits in a large molecule, such as amino acids in a peptide or protein (79,81) or sugar units in a carbohydrate (82).

The pulse sequence (Fig. 20) begins with a $\pi/2$ preparation pulse, after which the nuclei evolve during t_1. After t_1, an rf field (B_2) is switched on along the y axis in the rotating frame. The nuclei precess about this spin-lock field with the net effect that the y components of the magnetization vectors are "locked" along this field. The B_2 field is left on during the mixing period and J-coupled nuclei A and B interchange in-phase y magnetization at a rate dependent on J_{AB}.

$$\text{In-phase}_A \xrightarrow{\text{spin-lock rf field, } J_{AB}} \text{In-phase}_B$$

If the spin-lock field is left on for an extended period of time, the in-phase coherence transfer will continue to additional nuclei; the coherence that was transferred from nucleus A to nucleus B will, in turn, be transferred to nuclei that are J-coupled to B. For the most effective coherence transfer, it is essential that the amplitude of the rf field be strong enough to ensure that the two nuclei experience a B_2 field of the same intensity. They will then precess at the same frequency about B_2, becoming formally equivalent in the B_2 rotating frame [analogous to the Hartmann–Hahn match in solids (83)]. When this condition is satisfied, scalar coupling provides a mechanism for the exchange of in-phase magnetization. This exchange is termed "isotropic mixing" or "non-isotropic mixing" (cross-polarization) (77,84–87) depending on the nature of the pulse sequence used to generate the spin-lock.

In order that both of the coupled nuclei experience effective spin-lock fields that have the same intensity, resonance offset effects and rf inhomegeneity must be minimized. For this purpose, the most satisfactory spin-lock is achieved with schemes such as those mentioned above for ^{13}C decoupling in the ^1H-detected CH COSY experiment. These often consist of a series of relatively long composite π pulses (rf field strength corresponding to $\pi/2$ pulse width of ~50–100 μsec). The following phase cycle was used for obtaining HOHAHA spectra with TPPI.

	ϕ_1	ϕ_2	Ψ	
FID 1	x	y	x	Baseline offset removal
	$-x$	$-y$	$-x$	
FID 2	y	y	x	TPPI
	$-y$	$-y$	$-x$	
	.			
	.			
	etc.			

Scheme XIII

In the spectrum shown in Fig. 21, WALTZ-17 was used to generate the spin-lock. The WALTZ-16 portion of the spin-lock is a continuous series of x and $-x$ composite π pulses of the form $(\pi/2_x,\pi_{-x},3\pi/2_x)$ (57,58). WALTZ-17 is generated by adding a π_x uncompensated pulse at the end of the WALTZ-16 sequence as described by Bax and Davis for MLEV-17 (80). The WALTZ-17 sequence is repeated an integral number of times until the desired total spin-lock time is reached (actually, full compensation is achieved only when the WALTZ-17 sequence is repeated an even number of times). The entire sequence is preceded and followed by trim pulses. The function of the uncompensated π pulse and trim pulses is to remove small artifacts that accumulate during the repeated WALTZ-17 sequence. Spin-lock times of ca. 20 msec will produce cross-peaks mainly for directly coupled spins. Longer spin-lock times (up to ~120 msec) will result in more extended correlations. Any baseline DC offset

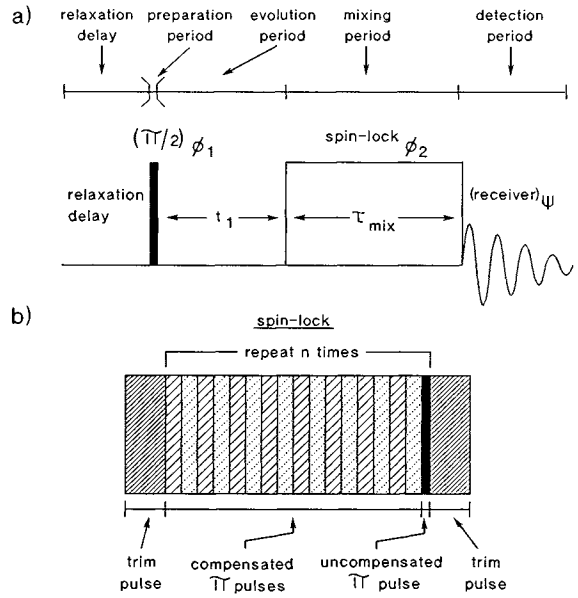

Fig. 20. (a) Pulse sequence used for 2D ROESY and TOCSY/HOHAHA showing (b) the details of the composite pulse spin-lock (WALTZ-17) used in TOCSY/HOHAHA.

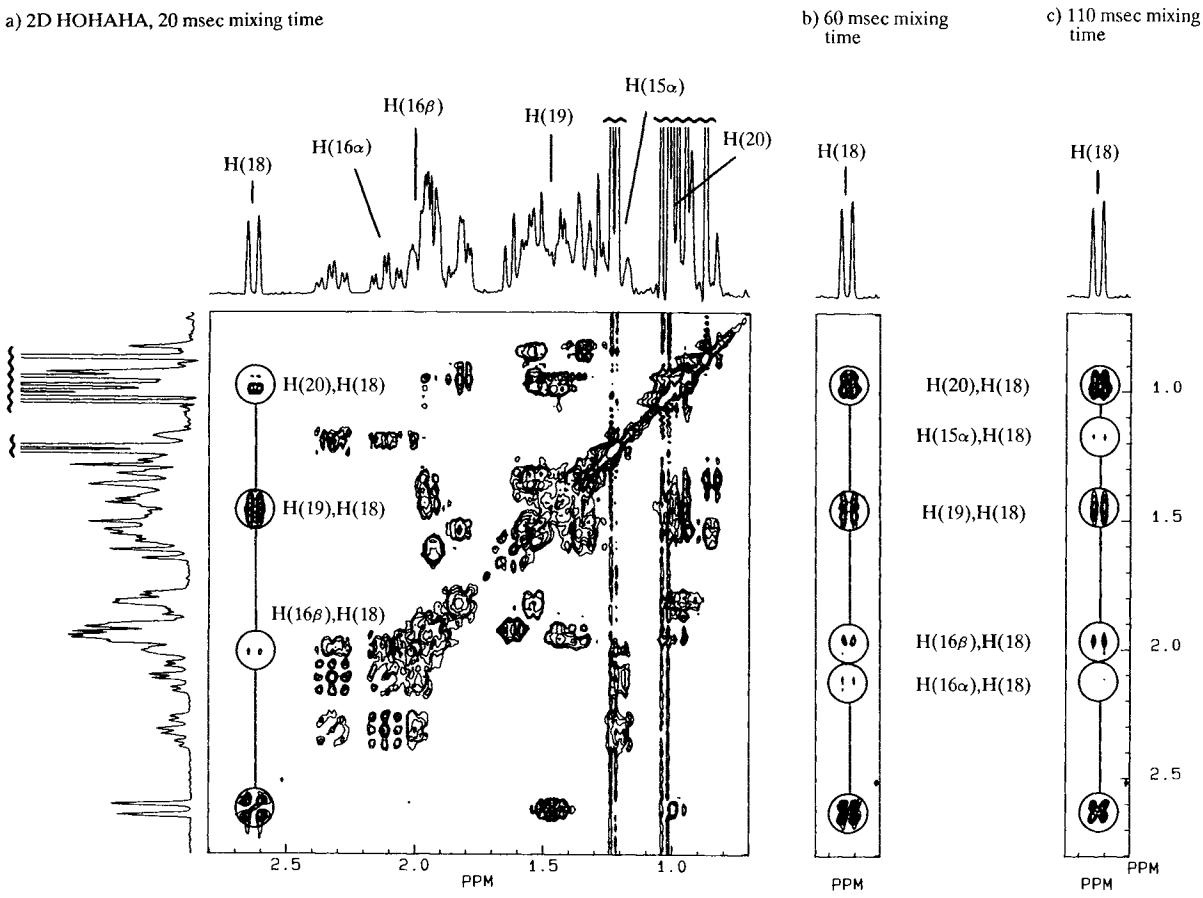

Fig. 21. 2D HOHAHA spectra of ursolic acid. TPPI acquisition; 512 (t_1) × 2048 (t_2) points, zero filled to 1024 × 2048; shifted ($\pi/3$) sine-bell apodization (both t_1 and t_2); pure-phase mode, only positive levels plotted. The width of the $\pi/2$ pulse used in the WALTZ sequence was 67.5 μsec; the trim pulses (2 msec) were of the same rf field strength. (a) Spectrum obtained with 20 msec mixing time, expansion of spectral region 0.7–2.8 ppm (ν_1)/0.7–2.8 ppm (ν_2); (b) spectrum obtained with 60 msec mixing time, expansion of spectral region 0.7–2.8 ppm (ν_1)/2.5–2.8 ppm (ν_2); (c) spectrum obtained with 110 msec mixing time, expansion of spectral region 0.7–2.8 ppm (ν_1)/2.5–2.8 ppm (ν_2). The dependence of cross-peak buildup on mixing time is illustrated for hydrogens coupled to H(18).

in the scans is canceled by phase alternating the two pulses and receiver in concert.

Shown in Fig. 21 are the HOHAHA spectra of 1 at three mixing times. As might be expected, many of the cross-peaks that appear in the 20 msec spectrum are duplicated in the COSY spectrum (Fig. 10), since both COSY and HOHAHA rely on J-coupling to produce cross-peaks. However, even at this short mixing time an additional weaker H(20),H(18) peak is observed that is not seen in the COSY spectrum. This peak results from relay through H(19). At longer mixing times the coherence transfer will propagate to additional nuclei, thereby providing a method for studying extended groups of coupled nuclei by utilizing the time dependence of cross-peak buildup. For example, in Figs. 21b and c, the H(20), H(18) peak becomes increasingly intense as the relay process continues, and an additional peak H(16α),H(18) appears. It is important to be aware that at longer mixing times (>ca. 100 msec), the HOHAHA spectrum can become contaminated with ROESY peaks.

Because of the many long-range couplings in 1, the HOHAHA spectrum does not produce the dramatic decomposition into sets of subspectra that is obtained when analyzing peptides or carbohydrates. In these molecules, there is almost no measurable intraresidue ^1H–^1H J-coupling, so that the spin systems of each residue (amino acid or sugar) are very effectively isolated.

The pulse sequence in Fig. 20a is used for both ROESY and TOCSY/HOHAHA. Therefore, the potential exists for ROESY peaks appearing in TOCSY/HOHAHA spectra, and vice versa. Even though these two types of cross-peaks are of opposite sign (Table I), they can overlap, causing mutual cancelation. Segregation of these two peak types can be accomplished by proper choice of spin-lock scheme, carrier offset, and mixing time. To minimize TOCSY/HOHAHA peaks in ROESY, it is important that a nucleus not experience a B_2 field of the same amplitude as that experienced by nuclei to which it is J-coupled, else in-phase coherence transfer will occur, and spectra will be contaminated with TOCSY/HOHAHA peaks. This is accomplished by using a relatively weak B_2 field (~2–5 kHz) (69–71), which will produce a larger offset dependence of effective spin-lock strength, and by locating the carrier at a frequency that is not equidistant between the chemical shifts of two J-coupled nuclei. A disadvantage of the weak spin-lock is that it produces

a significant offset-dependence in the intensity of cross peaks, resulting in diminished S/N.

Careful selection of mixing time allows minimization of ROESY peaks in TOCSY/HOHAHA spectra. During the mixing period, the ROESY peak buildup rate depends on the internuclear cross-relaxation time; if mixing times approach this cross-relaxation time (of the order of $T_{1\rho}$: rotating frame spin-lattice relaxation time), ROESY peaks will appear in the spectrum. Therefore, to minimize ROESY peaks in TOCSY/HOHAHA spectra, mixing times should be chosen with this restriction in mind. As mentioned above, research is not under way to establish methodology to eliminate peak cross-contamination in spin-lock experiments (69–71).

Summary

The complete ^1H and ^{13}C NMR assignments of ursolic acid are shown in Table II. They were obtained and confirmed by using and cross-correlating data from all the methods discussed above. As described in several reviews and texts (4–12,88,89), additional methods exist for obtaining spectral assignments and structural data. In general, the experiments that are chosen often reflect the type of molecule under investigation: for example, peptides and carbohydrates require long-range chemical shift correlation (both ^1H–^1H and ^{13}C–^1H) methods to establish interresidue connectivity through bonds; biomolecules studied in H_2O necessitate the use of solvent suppression; and biopolymers, which often have very broad resonances, require special techniques for measurement of coupling constants. There are several early 2D NMR experiments that are now used less frequently because either they provide information available from other experiments or they have limitations. Thus, we do not often use the commonly mentioned experiments such as 2D J-resolved spectroscopy (90), due to artifacts resulting from strong coupling and unreliability of coupling constant measurements, or 2D-INADEQUATE (91), due to the requirement for large amounts of sample, long experiment time, or high solubility.

CONCLUSION

In this Review we have discussed some of the critical factors that influence the acquisition, processing, and interpretation of 2D NMR spectra using some of the newer versions of the most useful methods. A strategy was presented for the structure elucidation of a complex molecule by 2D NMR. In the future, the spectroscopist will undoubtedly be faced with increasingly more complicated molecules and will, of necessity, rely heavily on newer NMR methodology. Concepts presented in this Review were aimed at providing access to current methodology as well as future developments.

REFERENCES

1. J. Jeener. Ampere International Summer School, Basko Polje, Yugoslavia (1971).
2. L. Müller, A. Kumar, and R. R. Ernst. *J. Chem. Phys.* **63**:5490–5491 (1975).
3. W. P. Aue, E. Bartholdi, and R. R. Ernst. *J. Chem. Phys.* **64**:2229–2246 (1976).
4. H. Kessler, M. Gehrke, and C. Griesinger. *Angew. Chem. Int. Ed. Engl.* 27:490–536 (1988).
5. R. Freeman. *A Handbook of Nuclear Magnetic Resonance,* John Wiley and Sons, New York, 1987.
6. J. H. Prestegard. In W. S. Brey (ed.), *Pulse Methods in 1D and 2D Liquid-Phase NMR,* Academic Press, New York, 1988, pp 435–488.
7. R. R. Ernst, G. Bodenhausen, and A. Wakaun. *Principles of Nuclear Magnetic Resonance in One and Two Dimensions,* Clarendon Press, Oxford, 1987.
8. K. Wüthrich. *NMR of Proteins and Nucleic Acids,* John Wiley and Sons, New York, 1986.
9. G. A. Morris. *Magn. Reson. Chem.* **24**:371–403 (1986).
10. A. Bax. *Bull. Magn. Reson.* 7:167–183 (1985).
11. G. Wider, S. Macura, A. Kumar, R. R. Ernst, and K. Wüthrich. *J. Magn. Reson.* **56**:207–234 (1984).
12. A. Bax. *Two-Dimensional Nuclear Magnetic Resonance in Liquids,* Delft University Press, Boston, 1982.
13. T. C. Farrar and E. D. Becker. *Pulse and Fourier Transform NMR,* Academic Press, New York, 1971.
14. D. M. Doddrell, P. W. Khong, and K. G. Lewis. *Tetrahedron Lett.* 2381–2384 (1974).
15. S. Seo, Y. Tomita, and K. Kai. *Tetrahedron Lett.* 7–10 (1975).
16. W. F. Reynolds, S. McLean, J. Poplawski, R. G. Enriquez, L. I. Escobar, and I. Leon. *Tetrahedron* **42**:3419–3428 (1986).
17. J. Jeener, B. H. Meier, P. Bachmann, and R. R. Ernst. *J. Chem. Phys.* 71:4546–4553 (1979).
18. C. P. Slicter. *Principles of Magnetic Resonance,* Springer-Verlag, New York, 1980, pp. 150–167.
19. O. W. Sørensen, G. W. Eich, M. H. Levitt, G. Bodenhausen, and R. R. Ernst. *Progr. NMR Spectrosc.* **16**:163–192 (1983).
20. A. Bax, R. Freeman, and G. A. Morris. *J. Magn. Reson.* **42**:164–168 (1981).
21. K. Nagayama, A. Kumar, K. Wüthrich, and R. R. Ernst. *J. Magn. Reson.* 40:321–334 (1980).
22. D. I. Hoult and R. E. Richards. *Proc. Roy. Soc. Lond. Ser. A* **344**:311–340 (1975).
23. A. D. Bain. *J. Magn. Reson.* **56**:418–427 (1984).
24. G. Bodenhausen, H. Kogler, and R. R. Ernst. *J. Magn. Reson.* **58**:370–388 (1984).
25. J. C. Lindon and A. G. Ferrige. *Progr. NMR Spectrosc.* **14**:27–66 (1980).
26. G. Bodenhausen, R. Freeman, R. Niedermeyer, and D. L. Turner. *J. Magn. Reson.* **24**:291–294 (1976).
27. P. Bachmann, W. P. Aue, L. Müller, and R. R. Ernst. *J. Magn. Reson.* 28:29–39 (1977).
28. A. Bax, R. Freeman, and G. A. Morris. *J. Magn. Reson.* **43**:333–338 (1981).
29. A. DeMarco and K. Wüthrich. *J. Magn. Reson.* **24**:201–204 (1976).
30. A. F. Mehlkopf, D. Korbee, T. A. Tiggleman, and R. Freeman. *J. Magn. Reson.* **58**:315–323 (1984).
31. G. A. Morris. *J. Magn. Reson.* 78:281–291 (1988).
32. R. E. Klevit. *J. Magn. Reson.* **62**:551–555 (1985).
33. G. Otting, H. Widmer, G. Wagner, and K. Wüthrich. *J. Magn. Reson.* **66**:187–193 (1986).
34. R. Baumann, G. Wider, R. R. Ernst, and K. Wüthrich. *J. Magn. Reson.* **44**:402–406 (1981).
35. L. Müller and R. R. Ernst. *Mol. Phys.* 38:963–992 (1979).
36. D. J. States, R. A. Haberkorn, and D. J. Ruben. *J. Magn. Reson.* **48**:286–292 (1982).
37. D. Marion and K. Wüthrich. *Biochem. Biophys. Res. Comm.* **113**:967–974 (1983).
38. J. Keeler and D. Neuhaus. *J. Magn. Reson.* **63**:454–472 (1985).
39. A. G. Redfield and S. D. Kunz. *J. Magn. Reson.* **19**:250–254 (1975).
40. R. R. Ernst. *Adv. Magn. Reson.* 2:1–135 (1966).
41. M. Gueron. *J. Magn. Reson.* 30:515–520 (1978).
42. U. Piantini, O. W. Sørensen, and R. R. Ernst. *J. Am. Chem. Soc.* 104:6800–6801 (1982).
43. G. A. Morris and R. Freeman. *J. Am. Chem. Soc.* **101**:760–762 (1979).
44. D. M. Doddrell, D. T. Pegg, and M. R. Bendall. *J. Magn. Reson.* 48:323–327 (1982).

45. A. A. Maudsley, L. Müller, and R. R. Ernst. *J. Magn. Reson.* 28:463–469 (1977).
46. G. Bodenhausen and R. Freeman. *J. Magn. Reson.* 28:471–476 (1977).
47. L. Müller. *J. Am. Chem. Soc.* 101:4481–4484 (1979).
48. A. Bax, R. H. Griffey, and B. L. Hawkins. *J. Magn. Reson.* 55:301–315 (1983).
49. D. H. Live, D. G. Davis, W. C. Agosta, and D. Cowburn. *J. Am. Chem. Soc.* 106:6104–6105 (1984).
50. A. Bax and S. Subramanian. *J. Magn. Reson.* 67:565–569 (1986).
51. D. Brühwiler and G. Wagner. *J. Magn. Reson.* 69:546–551 (1986).
52. M. R. Bendall and D. T. Pegg. *J. Magn. Reson.* 53:272–296 (1983).
53. G. Bodenhausen and D. J. Ruben. *Chem. Phys. Lett.* 69:185–189 (1980).
54. J. R. Garbow, D. P. Weitekamp, and A. Pines. *Chem. Phys. Lett.* 93:504–509 (1982).
55. A. Bax. *J. Magn. Reson.* 52:330–334 (1983).
56. M. H. Levitt and R. Freeman. *J. Magn. Reson.* 43:502–507 (1981).
57. A. J. Shaka, J. Keeler, T. Frenkiel, and R. Freeman. *J. Magn. Reson.* 52:335–338 (1983).
58. A. J. Shaka, J. Keeler, and R. Freeman. *J. Magn. Reson.* 53:313–340 (1983).
59. A. J. Shaka, P. B. Barker, and R. Freeman. *J. Magn. Reson.* 64:547–552 (1985).
60. R. Freeman, T. H. Mareci, and G. A. Morris. *J. Magn. Reson.* 42:341–345 (1981).
61. M. R. Bendall, D. T. Pegg, and D. M. Doddrell. *J. Magn. Reson.* 45:8–29 (1981).
62. M. R. Bendall, D. T. Pegg, D. M. Doddrell, and J. Field. *J. Magn. Reson.* 51:520–526 (1983).
63. D. Brühwiler and G. Wagner. *J. Magn. Reson.* 69:546–551 (1986).
64. A. Bax and S. Subramanian. *J. Magn. Reson.* 67:565–569 (1986).
65. J. H. Noggle and R. E. Schirmer. *The Nuclear Overhauser Effect, Chemical Applications*, Academic Press, New York, 1971.
66. S. Macura, Y. Huang, D. Suter, and R. R. Ernst. *J. Magn. Reson.* 43:259–281 (1981).
67. A. A. Bothner-By, R. L. Stephens, J. Lee, C. D. Warren, and R. W. Jeanloz. *J. Am. Chem. Soc.* 106:811–813 (1984).
68. A. Kalk and H. J. C. Berendsen. *J. Magn. Reson.* 24:343–366 (1976).
69. A. Bax and D. G. Davis. *J. Magn. Reson.* 63:207–213 (1985).
70. H. Kessler, C. Griesinger, R. Kerssebaum, K. Wagner, and R. R. Ernst. *J. Am. Chem. Soc.* 109:607–609 (1987).
71. C. Griesinger and R. R. Ernst. *J. Magn. Reson.* 75:261–271 (1988).
72. G. Eich, G. Bodenhausen, and R. R. Ernst. *J. Am. Chem. Soc.* 104:3731–3732 (1982).
73. P. H. Bolton and G. Bodenhausen. *Chem. Phys. Lett.* 89:139–144 (1982).
74. G. Wagner. *J. Magn. Reson.* 55:151–156 (1983).
75. A. Bax and G. Drobny. *J. Magn. Reson.* 61:306–320 (1985).
76. P. L. Weber and L. Müller. *J. Magn. Reson.* 73:184–190 (1987).
77. O. W. Sørensen. Dissertation, ETH, No. 7658 (1984).
78. L. Braunschweiler and R. R. Ernst. *J. Magn. Reson.* 53:521–528 (1983).
79. D. G. Davis and A. Bax. *J. Am. Chem. Soc.* 107:2820–2821 (1985).
80. A. Bax and D. G. Davis. *J. Magn. Reson.* 65:355–360 (1985).
81. P. L. Weber, L. C. Sieker, T. S. Anantha Samy, B. R. Reid, and G. Drobny. *J. Am. Chem. Soc.* 109:5842–5844 (1987).
82. D. G. Davis and A. Bax. *J. Am. Chem. Soc.* 107:7197–7198 (1985).
83. S. R. Hartmann and E. L. Hahn. *Phys. Rev.* 128:2042–2053 (1962).
84. N. Chandrakumar and S. Subramanian. *J. Magn. Reson.* 62:346–349 (1985).
85. N. Chandrakumar, G. V. Visalakshi, D. Ramaswamy, and S. Subramanian. *J. Magn. Reson.* 67:307–318 (1986).
86. N. Chandrakumar. *J. Magn. Reson.* 67:457–465 (1986).
87. N. Chandrakumar. *J. Magn. Reson.* 71:322–324 (1987).
88. G. Wider, S. Macura, A. Kumar, R. R Ernst, and K. Wüthrich. *J. Magn. Reson.* 56:207–234 (1984).
89. H. Kessler, W. Bermel, A. Müller, and K.-H. Pook. In S. Undenfriend, J. Meienhofer, and V. J. Hruby (eds.), *The Peptides, Vol. 7*, Academic Press, New York, 1985, pp. 437–473.
90. W. P. Aue, J. Karhan, and R. R. Ernst. *J. Chem. Phys.* 64:4226–4227 (1976).
91. A. Bax, R. Freeman, T. A. Frenkiel, and M. H. Levitt. *J. Magn. Reson.* 43:478–483 (1981).